Vol. 01 No. 03 2023

RiESTech

JOURNAL RECENT IN ENGINEERING SCIENCE AND TECHNOLOGY

MBI

E- ISSN : 2985-8321
P -ISSN : 2985-704X

Recent in Engineering Science and Technology (RiESTech)
PT MENCERDASKAN BANGSA INDONESIA (MBI)
Available online at: http://www.mbi-journals.com/index.php/riestech

E- ISSN : 2985-8321
P -ISSN : 2985-704X

Recent in Engineering Science and Technology (RiESTech)

Volume 1 No 3 July 2023

FOCUS AND SCOPE

RIESTECH

Recent in Engineering Science and Technology **(RiESTech):** I*SSN: 2985-704X (print), ISSN: 2985-8321 (online)* a peer-reviewed quarterly engineering journal, publishes theoretical and experimental high-quality papers to promote engineering and technology's theory and practice. In addition to peer-reviewed original research papers, the Editorial Board welcomes original research reports, state-of-the-art reviews, and communications in the broadly defined field of recent engineering science and technology. **RiESTech** covers topics contributing to a better understanding of engineering, material science, computer science, environmental science, and their applications. **RiESTech** is concerned with scientific research on mechanical and civil engineering, Electrical/Electronics and Computer Engineering, and Metallurgical and Materials Engineering with specific analytical techniques and/or computational methods.

The frequency of RiESTech publications is four times a year namely in January, April, July, and October. The scope of RiESTech includes a wide spectrum of subjects namely:

Mechanical and Civil Engineering (Automotive Technologies; Construction Materials; Design and Manufacturing; Dynamics and Control; Energy Generation, Utilization, Conversion, and Storage; Fluid Mechanics and Hydraulics; Heat and Mass Transfer; Micro-Nano Sciences; Renewable and Sustainable Energy Technologies; Robotics and Mechatronics; Solid Mechanics and Structure; Thermal Sciences)

Electrical/Electronics and Computer Engineering (Instrumentation; Coding, Cryptography, and Information Protection; Communications, Networks, Mobile Computing, and Distributed Systems; Compilers and Operating Systems; Parallel Processing, and Dependability; Computer Vision and Robotics; Control Theory; Electromagnetic Waves, Microwave Techniques and Antennas; Embedded Systems; Integrated Circuits, VLSI Design, Testing, and CAD; Microelectromechanical Systems; Microelectronics, and Electronic Devices and Circuits; Power, Energy and Energy Conversion Systems; Signal, Image, and Speech Processing; Machine Learning and Data Science)

E- ISSN : 2985-8321
P -ISSN : 2985-704X

Metallurgical and Materials Engineering (Advanced Materials Science; Ceramic and Inorganic Materials; Electronic-Magnetic Materials; Energy and Environment; Materials Characterization; Metallurgy Extractive; Polymers and Nanocomposites)

Environmental Science and Engineering (Waste Management, Climate Change, Zero Waste, Environmental Disaster Management, Circular Economy, Sustainable Development, Environmental Security, Environmental Management, Environmental Ecology, Conservation of Natural Resources And Environment, Environmental Impact Analysis, Planning and Environmental Administration, Environmental Health, Environmental Pollution, Environmental Accounting, and Environmental Information Systems)

Recent in Engineering Science and Technology (RiESTech)
PT MENCERDASKAN BANGSA INDONESIA (MBI)
Available online at: http://www.mbi-journals.com/index.php/riestech

E- ISSN : 2985-8321
P -ISSN : 2985-704X

Recent in Engineering Science and Technology

(RiESTech)

Volume 1 No 3 July 2023

Recent in Engineering Science and Technology (RiESTech)
PT MENCERDASKAN BANGSA INDONESIA (MBI)
Available online at: http://www.mbi-journals.com/index.php/riestech

E- ISSN : 2985-8321
P -ISSN : 2985-704X

Layout and Typesetting:
Imam Sapto Nugroho, Universitas Indonesia (Alumni), Indonesia
Kamil Raihan Permana, Universitas Indonesia, Indonesia
Raihan Trinanda Agsya, Politeknik Negeri Jakarta, Indonesia

PUBLISHER
PT MENCERDASKAN BANGSA INDONESIA (MBI)
Address : 4th Floor Gedung STC Senayan Room 31-34, Jl. Asia Afrika Pintu IX, Jakarta 10270, Indonesia.

Recent in Engineering Science and Technology (RiESTech)
PT MENCERDASKAN BANGSA INDONESIA (MBI)
Available online at: http://www.mbi-journals.com/index.php/riestech

E- ISSN : 2985-8321
P -ISSN : 2985-704X

Recent in Engineering Science and Technology (RiESTech)

Volume 1 No 3 July 2023

PREFACE

Journal RiESTech (p-ISSN: 2985-704X (print), e-ISSN: 2985-8321 (online); is a peer review journal published by PT Mencerdaskan Bangsa Indonesia. The RiESTech journal is published four times a year in January, April, July, and October. This journal provides direct open access to its content on the principle that making research freely available to the public supports a greater global exchange of knowledge within the engineering field. This journal aims to provide a place for academics, researchers, and practitioners to publish original research articles or review articles. The scope of articles published in this journal relates to various topics in the field of outcomes of research activities.

The RiESTech journal publishes papers strictly following the RiESTech guidelines and templates for manuscript preparation. All submitted manuscripts will go through a double-blind peer review process. The paper is read by members of the editor (according to the area of specialization) and will be screened by the Managing Editor to meet the criteria required for RiESTech publication. Manuscripts will be sent to two reviewers based on their historical experience in reviewing manuscripts or based on their areas of specialization. RiESTech has review forms to keep the same item reviewed by two reviewers. Then the editorial board makes a decision on the comments or suggestions of the reviewers.

Reviewers provide an assessment of originality, clarity of presentation, contribution to the field/science. This journal publishes research articles, review articles/literature reviews, case reports and concept/policy articles, in all fields of Computer Science, Informatics Engineering, Multimedia, Arts. The article to be published is an original work and has never been published. Incoming articles will be reviewed by the reviewer team.

The Editorial Board will try to continue to improve the quality of the journal so that it can become an important reference in the development of engineering sciences. The greatest appreciation and gratitude to Mitra Bestari along with members of the Editorial Board and all parties involved in the publication of this journal. Complete writing instructions are displayed on the portal of this journal.

Regards,

Chief Editor

Recent in Engineering Science and Technology (RiESTech)
PT MENCERDASKAN BANGSA INDONESIA (MBI)
Available online at: http://www.mbi-journals.com/index.php/riestech

E- ISSN : 2985-8321
P -ISSN : 2985-704X

Recent in Engineering Science and Technology (RiESTech)

Volume 1 No 3 July 2023

Contents

Articles

RiESTech
Recent in Engineering Science and Technology

MBI

Article

Effect of Slope Chute Angle of HAP Magnetic Separator to the Acquisition of Nickel Matte from Undersized Product Resulted by Pierce Smith Converter Machine

Nurhayati Indah Ciptasari[1], Egidius Arya Parande[1], Johny Wahyuadi Soedarsono[1], Agus Budi Prasetyo[2], Wahyu Mayangsari[2], Reza Miftahul Ulum[1], Ahmad Maksum[3,*]

[1] Department of Metallurgical and Materials Engineering, Universitas Indonesia, Depok, Indonesia
[2] Research Center for Metallurgy and Materials - Indonesian Institute of Sciences, Kawasan PUSPITEK Gedung 470, Tangerang Selatan
[3] Department of Mechanical Engineering, Politeknik Negeri Jakarta, Depok 16425, Indonesia
* Correspondence: ahmad.maksum@mesin.pnj.ac.id

Abstract: The prototype of a magnetic separator was initiated and manufactured for handling undersized products of Pierce Smith Converter which has been channeled to a temporary shelter called a matte pond. It was dredged three to four times a year and it's costly. This expenditure can be minimized by the manufacture of magnetic separators that used to attract undersized nickel products. The manufacture of this prototype uses a scale of 1:20.000 for the volume of water and nickel matte, while for chute and magnetic drums with a scale of 1:4 from the conditions in the field. The purpose of this research is to find out whether magnetic separators are relevant for installation in the nickel processing industry, with the slope angle of the chute and magnetic power as the main parameters. Thus the matte pond can be minimized and undersized products can be directly processed and distributed to consumers. The material used in the manufacture of this prototype is aluminum sheet 1/16 in which is rolled for magnetic drums, aluminum sheet 1/8 in for chute, copper wire 0.5 mm and mild steel, lathe for rods and axis, and bending for magnetic holders. The result of this magnetic separator prototype is 24.48% nickel can be attracted.

Keywords: Magnetic Separator; Nickel Matte; Undersized Product; Pierce Smith

Citation: Indah Ciptasari, N., Arya Parande, E., Wahyuadi Soedarsono, J., Budi Prasetyo, A., Mayangsari, W., Miftahul Ulum, R., & Maksum, A. (2023). Effect of Slope Chute Angle of HAP Magnetic Separator to the Acquisition of Nickel Matte from Undersized Product Resulted by Pierce Smith Converter Machine. Recent in Engineering Science and Technology, 1(03), 1–12. https://doi.org/10.59511/riestech.v1i03.18

Academic Editor: Iwan Susanto

Received: 8 May 2023
Accepted: 29 May 2023
Published: 1 July 2023

Publisher's Note: MBI stays neutral with regard to jurisdictional claims in published maps and institutional affiliations.

1. Introduction

Nickel is one of the abundant minerals in Indonesia, especially on the island of Sulawesi, which has made many nickel mining processing plant [1]. Metallic nickel and nickel compounds are used in manifold industrial and commercial applications such as batteries, coinage, catalysts, electronics, pigments, stainless steel and other nickel alloys, electroplating, foundries, and ceramics [2]. Nickel is produced from two main sources: sulfide ore and laterite ore. While 70% of land-based nickel resources are contained in laterite deposits, the majority of the world's nickel production currently still comes from sulfide sources. The dominant nickel mineral in these deposits is pentlandite (NiFe)9S8 this is because the main mineral of nickel sulfide ore is pentlandite [3], [4].

Previous researchers have tried to increase nickel concentration through a reduction process [5]–[8], using either coal [9], [10] or natural reducing agents such as palm kernel shell [11]–[15], rice husk [16], [17], coconut [18], [19], and bagasse [20]. In one of

the mining industries in Sulawesi, there was a problem in the process of handling undersized products from the nickel matte granulation process from the refining process in the Pierce-Smith Converter. In general, the process that occurs from Pierce-Smith Converter to produce products that are ready to be packaged is illustrated in Figure 1.

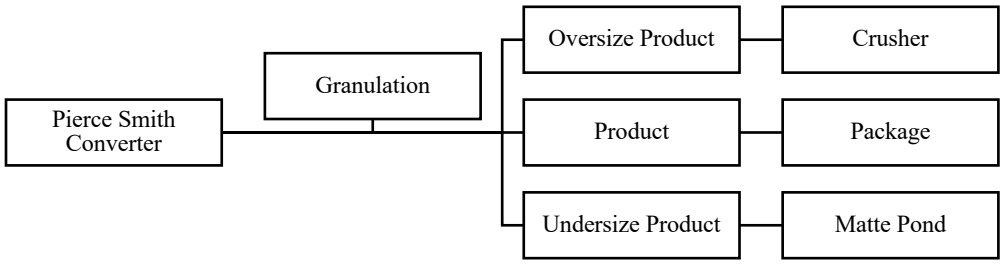

Figure 1. General Process Flow Diagram in Converter [4].

From Figure 1, it can be seen that from the granulation process or casting converter matte to matte granule, three product sizes were produced can be categorized as :

1. Oversize products or products with a size larger than consumer demand which will later be processed with a crusher to obtain products according to qualifications and returned to the granulation process
2. Products in accordance with consumer demand
3. Undersize products or products smaller than 100 mesh that has been channeled into temporary storage ponds called matte ponds that are reclaimed three to four times a year, and sump pits are clamping once a month to take small nickel grains that are accommodated in that area.

The pouring on the granulation system is a very important part where the poured matte liquid will become a matte granule [4], [21]. There are no parameters used to determine the size of the granulation product, only a visual observation and requires sufficient experience, therefore three types of products are formed as shown in Figure 1. Responding to this, the idea arose for handling undersize products more effectively and efficiently. The idea is illustrated in the scheme in Figure 2.

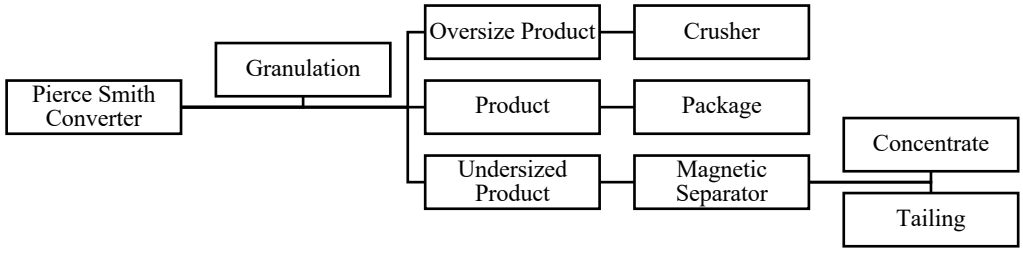

Figure 2. New Flow Chart Offer in Pierce-Smith Converter.

The innovation in this research is to replace the matte pond with a magnetic separator for handling undersized products from the granulation process. With the magnetic separator, it is expected that the undersized product from the granulation process can be handled more effectively, efficiently, and increase the productivity of nickel.

2. Materials And Methods

This research was conducted with a HAP magnetic separator by flowing a mixture of nickel matte with water, hereinafter referred to as slurry from slurry drum to the magnetic drum by passing through the chute with a certain slope. In this research, we will find the optimum slope chute angle to get the maximum efficiency. The tools and materials in this research are adjusted to the industrial scale because it is hoped that the results of this study can be scaled up to industrial scale. The nickel matte used in this study is the undersized product of granulation from Pierce Smith Converter whose sizes range from 100 - 400 mesh. In addition, the research will also find out the size distribution of nickel matte so that later it can be seen on the size of how dominant the particles are magnetized and on how many particles are lost or loss. In addition, to find out the composition of the sample that will be examined in advance the sample will be tested with XRF and the final product too. To calculate the efficiency of nickel matte in this study were calculated with a dry-based product. The final goal of this research is that the magnetic separator can be developed from a prototype scale into an industrial-scale tool to help nickel industries to be able to increase its productivity.

Materials :

1. Undersized product of nickel matte from granulation process of the Pierce Smith Converter with sizes ranging from 100 - 400 mesh
2. Mild steel st. 37 solid cylindrical shape which is turned to become a magnetic drum, magnetic rod, and sheet supporting shaft for magnetic rod mounting applications.
3. Aluminum Alloy 6061, sheet-thickness 0.063 in (1/16 in) for magnetic drum blankets and sheet-thickness 0.125 in (1/8 in) for chute, product storage containers, and disposal systems.
4. 0.5mm copper wire for electrical conductor winding wire on each magnetic rod.
5. Water to be mixed with nickel matte to make it slurry like the conditions in the field.

Parameters: Effect of slope chute, variation at an angle of 15, 20, and 25 deg to the efficiency of undersized nickel matte.

This experiment is limited by assuming the fluid flow is considered constant and laminar, there is no friction between the slurry and the chute where the slurry flows, the process of agitation is considered constant, magnetic drum rotation is considered constant, and the study was conducted on a prototype scale with a certain scale.

3. Results And Discussion

Previous research with HAP magnetic separator obtained 2.4% recovery using product-based calculations. Further research on HAP Magnetic separator was carried out because the efficiency of previous research was still very low, with the hope of getting efficiency of undersized nickel product in the nickel industry in Sulawesi which is higher. The evaluation of the previous HAP magnetic separator was that there were no product storage containers, the slope chute angle was not set and changed every trial, the tailings disposal system was not organized so that it polluted the surrounding environment, and the magnetic drum blanket was still thick due to using aluminum alloys 6061 sheet-thickness 1/8 inch or 0.125 inch. This evaluation tool is used as a benchmark to make HAP magnetic separators more efficient in terms of process and efficiency.

The following will describe the data and operational conditions collected through literature, direct experiments, and also field observations used to support this research. The operational data used is sourced from the Metal Accounting division one of the nickel industry in Sulawesi which includes undersized matte pond reclaim data and matte pond sieve analysis data. Table 1 summarizes the reclaimed matte pond data from May 2018 to February 2019 obtained from the Metal Accounting division :

Table 1. Data Reclaim Undersized Product (Matte Pond)

No.	Period	Ni Weight (Ton)	Unit
1.	May–August	104.55	DMT
2.	August–November	124.30	DMT
3.	November–February	123.92	DMT
	Total	**352.77**	

From the data in Table 1, it can be seen that the reclaim for nine months, from May 2018 to February 2019 is 352.77 Dry Metric Ton (DMT) and if averaged per month there are 39.19 DMT of undersized nickel products entering into the matte pond, if multiplied by a year, there are 470 DMT of undersized products that are accommodated in the matte pond and must wait for their turn to be reclaimed so that later they can produce value which is further diminished by reclaiming operational costs to pay labor and heavy equipment to become profit.

To find out the sample size distribution that will be used for the research process, sieve analysis is carried out using a sieve shaker with sieves of 100 mesh, 200 mesh, 230 mesh, 325 mesh, and 400 mesh respectively.

Table 2. Sieve Distribution Data of Matte Pond Feed.

Particle Size (mesh)	Weight (gr)	Persentage (%)
- 100	3.8	0.76
+ 100 – 140	14.6	2.92
+ 140 – 200	76.8	15.36
+ 200 – 230	88.2	17.64
+ 230 – 325	103.4	20.68
+ 325 – 400	160.2	32.04
- 400	49.6	9.92
loss	3.4	0.68

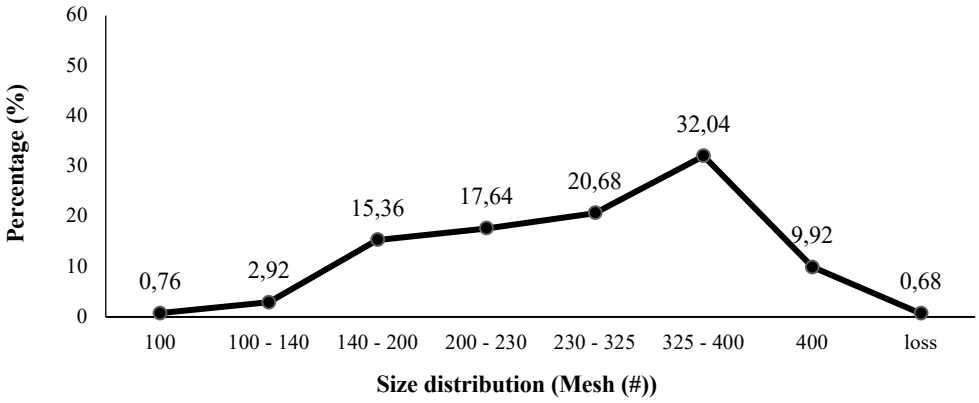

Figure 3. Distribution of Matte Pond Feed Particles.

The operational data sieve analysis of the undersized product sample in Figure 3 shows the distribution of particles in the matte pond or temporary storage pond for undersized products. Based on Table 2 and the illustration in the graph in Figure 3, the sample tendency to be tested is at most 325-400 mesh or around 44-37 micron (μm) 32.04%, and at least at 100 mesh or 149 micron (μm)) the amount is 0.76%. These particles will be used as sample experiments in this study.

Table 3. Composition of mineral elements in the product and the tailings.

No	Sample	Slope of the chute	Electric Current (A)	Composition			
				Ni (%)	Fe (%)	Co (%)	S (%)
1.	Product *Matte Pond*	25 deg	3.75	78.81	0.594	1.098	19.4
2.	*Tailing Matte Pond*	25 deg	3.75	79.24	0.666	1.094	18.9
3.	Product *Matte Pond*	20 deg	3.75	79.19	0.651	1.052	19.1
4.	*Tailing Matte Pond*	20 deg	3.75	79.14	0.671	1.094	19.0
5.	Product *Matte Pond*	15 deg	3.75	79.24	0.617	1.075	19.06
6.	*Tailing Matte Pond*	15 deg	3.75	78.82	0.698	1.085	19.2
7.	Product *Matte Pond*	15 deg	3.0	78.97	0.533	1.101	19.3
8.	*Tailing Matte Pond*	15 deg	3.0	78.92	0.681	1.101	19.2
9.	Product *Matte Pond*	15 deg	2.25	79.04	0.578	1.087	19.2
10.	*Tailing Matte Pond*	15 deg	2.25	78.92	0.691	1.094	19.2

The XRF data from the laboratory is shown in Table 3, it can be seen the composition of mineral elements in the product and the tailings of the experimental results shown are the elements Ni, Fe, Co, and S, it is possible there are still other elements. However, the data in Table 3 only shows the most dominant elements contained in the product and tailings in this experiment. The data in Table 3 is also still influenced by the variable slope of the chute and the magnetic strength.

To optimize the process, the slope of the chute at a certain point is needed to get an efficient process. The slope of the chute will affect the flow rate, productivity, and of course the effect on efficiency in this study. Therefore, determining the optimum point of the slope chute angle in this experiment is very important because it supports almost all lines. In this research, the chute serves as a slurry distribution medium from the slurry drum to the magnetic drum. Chute referred to here is an artificial channel made of aluminum with a length of 157cm and width of 37.4cm. The reason for choosing aluminum as the materials of the chute is because aluminum is easily fabricated and strong enough to accept low fluid flows [22]. In addition, if the material used is iron, iron tends to have ferromagnetic properties and can be attracted strongly by magnets, it is feared that when using iron, magnets will also attract the chute so that the magnet does not focus on attracting the slurry being flowed. Calculation of the length and width of the chute has been adjusted to the magnetic drum holder, besides that there is also a chute holder that functions as a supporting chute. With the chute holder, the slope angle of the chute can be adjusted according to the desired slope and this slope variation will be examined in this study to later obtain the optimum angle that supports maximum efficiency

Actually not only limited to the slope chute angle to get the optimum efficiency, however, the design process and also fabrication must be made and thought out into separate parts and can become a single unit so that the links between these parts can be drawn [23]. However, the focus in this study will look at the influence of the slope chute angle which is a very influential thing in terms of the productivity of devices such as magnetic separators. The following will describe the results of experiments that have been carried

out by using a variation of slope chute at an angle of 15, 20, and 25 deg to the efficiency of matte nickel, with the condition of the HAP magnetic separator, made standard using 112.5W electrical power, 3.75A input current, and 30V voltage using a sample of nickel undersized products that have been prepared.

Experiment with the sloping chute at an angle of 15 deg

Table 4 shows the experimental results with the sloping chute at an angle of 15 deg.

Table 4. Experiment results with the sloping chute at an angle of 15 deg.

Current (A)	Feed (kg)	Product (kg)	Tailing (kg)	efficiency (Product Base) (%)	efficiency (Tailing base) (%)
3.75	16	4.678	9.100	29.23	56,87
3.75	16	3.032	8.180	18.95	51,12
3.75	16	4.046	10.468	25.28	65,42
Average		3.918	9.25	24.48	57.80

From the data in Table 4 it can be seen that from the 16kg samples tested an average of 3.91kg became products and calculated as efficiency product base, if calculated in percent counts there was an average of 24.48% of samples that could be attract by HAP magnetic separator. While for tailings from samples weighing an average of 9.25 kg which is calculated as efficiency of tailing base, if calculated in percent counts there is an average of 57.80% of samples that become tailings in this experiment. This tailing rate is quite high because of the limited power that can be provided by the power supply and also the agitation system which is still made manually, thus making many samples left at the bottom of the slurry drum. To find out the distribution of particles that can be attract into products and tailings, a sieve analysis is conducted for the results of this experiment, the distribution data is shown in Table 5.

Table 5. Matte Pond Sieve Analysis Results, sloping chute at an angle of 15 deg.

Size (mesh)	Product (514 gr)		Tailing (500 gr)	
	Weight (gr)	Percentage (%)	Weight (gr)	Percentage (%)
- 100	1.6	0.31	1.9	0.3
+ 100 – 140	7.7	1.50	6.9	1.38
+ 140 – 200	50.8	9.88	43.2	8.64
+ 200 – 230	80.1	15.58	99.6	19.92
+ 230 – 325	182.9	35.58	240.4	48.08
+ 325 – 400	61.3	11.93	2.5	0.5
- 400	127.1	24.73	103.2	20.6
Loss	2.5	0.49	2.3	0.46

The sample used to carry out this sieve analysis is a sample that has been homogenized and taken approximately 500gr to be further tested on a sieve shaker machine to determine its size distribution. It can be seen that the most particles into a product are +230 - 325 mesh particles which are 182.9gr or 35.58% for products and particles +230 - 325 mesh which are 240.4gr or 48.08% for tailings, this is influenced because the second largest number of particles in the sample makes it possible to recover more and become tailings simultaneously.

Experiment with the sloping chute at an angle of 20 deg

Table 6 shows the experimental results with the sloping chute at an angle of 20 deg.

Table 6. Experiment results with the sloping chute at an angle of 20 deg.

Current (A)	Feed (kg)	Product (kg)	Tailing (kg)	efficiency (Product Base) (%)	efficiency (Tailing base)(%)
3.75	16	2.854	9.588	17.83	59,92
3.75	16	2.302	12.846	14.38	80,28
3.75	16	3.890	12.566	24.31	78,53
Average		3.015	11.667	18.84	72.91

In Table 6 it can be seen that from the 16 kg samples tested, an average of 3.01 kg became a product and was calculated as efficiency product base. While for tailings from samples weighing an average of 11.66 kg which is calculated as the efficiency of tailing base, if calculated in percent counts there is an average of 72.91% of samples that become tailings in this experiment. This tailing rate is quite high because there is an increase in the angle of 5o, the limited power that can be provided by the power supply and also the agitation system which is still made manually, thus making many samples left at the bottom of the slurry drum and the slope of the chute high enough to make the slurry flow with very fast and makes the magnetic drum time to attract samples so short that many samples become tailings. To find out the distribution of particles that can be attract into products and tailings, a sieve analysis is conducted for the results of this experiment, the distribution is shown in Table 7.

It is known that the particles which are the most widely produced are particles of +230 - 325 mesh in the amount of 155.5gr or 31.1% and for tailings the same thing is obtained, where the particles most attracted by magnets are particles sized +230 - 325 mesh as many as 219.6gr or 43.92% of the total particles that become tailings. This is influenced because the number of particles measuring +230 - 325 mesh is the most in the sample so that it is possible to recover more and become tailings simultaneously.

Table 7. Matte Pond Sieve Analysis Results, sloping chute at an angle of 20 deg.

Size (mesh)	Product (504 gr)		Tailing (500 gr)	
	Weight (gr)	Percentage (%)	Weight (gr)	Percentage (%)
- 100	1.9	0.38	2.2	0.44
+ 100 – 140	8.0	1.60	8.4	1.68
+ 140 – 200	57.9	11.58	61	12.20
+ 200 – 230	95.7	19.14	122.7	24.54
+ 230 – 325	155.5	31.10	219.6	43.92
+ 325 – 400	37	7.40	28.5	5.70
- 400	146.8	29.36	57.6	11.52
Loss	2	0.24	0	0

Experiment with the sloping chute at an angle of 25 deg

Table 8 shows the experimental results with the sloping chute at an angle of 25o.

Table 8. Experiment results with the sloping chute at an angle of 25 deg.

Current (A)	Feed (kg)	Product (kg)	Tailing (kg)	efficiency (Product Base) (%)	efficiency (Tailing base) (%)
3.75	16	2.534	10.214	15.83	63.83%
3.75	16	2.338	9.878	14.61	61.73%
3.75	16	2.376	10.360	14.85	64.75%
Average		2.416	10.159	15.09	63.43%

Table 8 shows that out of the 16 kg samples tested. an average of 2.416 kg became a product and was calculated as efficiency product base. if calculated in percent counts there was an average of 15.09% of samples that could be attract by HAP magnetic separator. While for tailings from samples weighing an average of 10.15 kg which is calculated as the efficiency of tailing base. if calculated in percent counts there is an average of 63.43% of the samples that become tailings in this experiment. This tailing rate is the highest when compared to the other slope. Same as the situation in the two previous experiments this was due to the limited power that could be provided by the power supply and also the agitation system which was still made manually. One important point of the low efficiency in experiments with the sloping chute at an angle of 25o is due to the increase in slope which is quite far compared to other variables and variables recommended by some of the literature. As a result. experiments with sloping chute at an angle of 25o make the slurry flow very quickly and make the magnetic drum time to attract the sample very short so that many samples become tailings. To find out the distribution of particles that can be attract into products and tailings. a sieve analysis is conducted for the results of this experiment. the distribution is shown in Table 9.

Table 9. Matte Pond Sieve Analysis Results. sloping chute at an angle of 25 deg.

Size (mesh)	Product (500 gr)		Tailing (500 gr)	
	Weight (gr)	Percentage (%)	Weight (gr)	Percentage (%)
- 100	2.3	0.46	2.1	0.42
+ 100 – 140	13.1	2.62	9.6	1.92
+ 140 – 200	79.6	15.92	51.1	10.22
+ 200 – 230	92	18.4	76	15.20
+ 230 – 325	185.7	37.14	225.7	45.14
+ 325 – 400	29.5	5.90	95.3	19.06
- 400	78.2	15.64	35.6	7.12
Loss	19.6	3.92	4.6	0.92

It is known that the particles which are the most widely produced are particles of +230 - 325 mesh in the amount of 185.7gr or 37.14% and for tailings the same thing is obtained. where the particles most attracted by magnets are particles sized +230 - 325 mesh as many as 225.7gr or 45.14% of the total particles that become tailings. this is influenced because the number of particles of that size is the most in the sample so it is possible to recover more and become tailings simultaneously

4. Conclusions

The most optimum slope of the chute results of this study is 15o. The greater the slope angle. the higher the flow rate. high productivity. but will reduce efficiency. so the efficiency is low. If the chute angle is low. the efficiency is high. but the production capacity is low and the optimum value of the slope of the chute is 15°. The biggest average of efficiency obtained from this study was 24.48%. far greater than the previous research results of 2.4%. In this study. the most dominant particle size of the sieve analysis results in size +230 - 325 mesh. Particles of this size are the most products or tailings in this experiment. With the presence of HAP Magnetic Separator for handling undersized products. with 24.48% efficiency.

5. Acknowledgment

The authors sincerely acknowledge the fundings to this research work from PT. Vale Indonesia. Tbk and Universitas Indonesia under PIT9 Research Grants with Contract No. NKB–0062/UN2.R3.1/HKP.05.00/2019. and the fabrications of HAP magnetic separator assistance by Akademi Teknik Soroako.

References

1. E. H. Sujiono. M. Diantoro. and Samnur. "The physical properties of nickel ore in Sorowako South Sulawesi." *J. Pendidik. Fis. Indones.*. vol. 10. no. June 2015. pp. 163–167. 2014.
2. W. S. Tait. "Controlling corrosion of chemical processing equipment." in *Handbook of Environmental Degradation Of Materials: Third Edition*. Third.. 2018. pp. 583–600.
3. D. Schaumlöffel. "Nickel species: Analysis and toxic effects." *J. Trace Elem. Med. Biol.*. vol. 26. no. 1. pp. 1–6. 2012.

4. J. R. Lawang. *Pierce Smith Converter Operation*. PT. INCO HRD & Training. 2004.
5. J. W. Soedarsono. R. Simarmata. A. Kawigraha. R. D. Sulamet-Ariobimo. A. Rustandi. S. Tjahyono. and A. Zamri. "Effect of reduction process parameter in direct reduction process of laterite to produce substitute pig iron for thin wall ductile iron material." *Adv. Mater. Res.*. vol. 893. pp. 95–99. 2014.
6. R. H. Pangaribuan. J. Patrick. A. B. Prasetyo. A. Maksum. and B. Munir. "The effect of NaOH (natrium hydro.xide) to slag nickel pyrometallurgy in different temperature and additive ratio." *E3S Web Conf.*. vol. 67. p. 03052. 2018.
7. S. Harjanto and M. A. Rhamdhani. "Sulfides formation in carbothermic reduction of saprolitic nickel laterite ore using low-rank coals and additives: A thermodynamic simulation analysis." *Minerals*. vol. 9. no. 10. 2019.
8. Z. Zulhan and I. Gibranata. "Direct reduction of low grade nickel laterite ore to produce ferronickel using isothermal – temperature gradient." *AIP Conf. Proc.*. vol. 1805. no. 040003. pp. 040003-1–9. 2017.
9. Yudianto. A. Maksum. Delfiendra. and J. W. Soedarsono. "Effects of temperature on the direct reduction of Southeast Sulawesi's limonite ore." *IOP Conf. Ser. Earth Environ. Sci.*. vol. 105. no. 1. p. 012066. 2017.
10. S. Suman and S. Gautam. "A comparative study between time. temperature. and fixed carbon using different biochar reductants as an alternate source of energy." *Energy Sources. Part A Recover. Util. Environ. Eff.*. vol. 39. no. 10. pp. 1029–1035. 2017.
11. S. Adzhani. R. Hidayanti. A. Maksum. S. Permana. and J. W. Soedarsono. "The influence of palm kernel shell mass ratio as a reducing agent in the lateritic nickel ore carbothermic reduction process." in *IOP Conference Series: Earth and Environmental Science*. 2017. vol. 105. no. 1. p. 012016.
12. D. Rahayu. A. Maksum. and J. W. Soedarsono. "Effects of reduction time on carbothermic reduction of lateritic nickel ore using palm kernel shell as green reducing agent." *IOP Conf. Ser. Earth Environ. Sci.*. vol. 105. no. 1. p. 012037. 2017.
13. B. Suharno. N. P. Ilman. A. Shofi. D. Ferdian. and F. Nurjaman. "Study of low-grade nickel laterite processing using palm shell charcoal as reductant." *Mater. Sci. Forum*. vol. 1000 MSF. no. 2010. pp. 436–446. 2020.
14. R. Z. Abd Rashid. H. Mohd. Salleh. M. H. Ani. N. A. Yunus. T. Akiyama. and H. Purwanto. "Reduction of low grade iron ore pellet using palm kernel shell." *Renew. Energy*. vol. 63. pp. 617–623. 2014.
15. E. Sugiarto. A. D. P. Putera. and H. T. B. M. Petrus. "Kinetic study of nickel laterite reduction roasting by palm kernel shell charcoal." *IOP Conf. Ser. Earth Environ. Sci.*. vol. 65. no. 1. 2017.
16. A. Maksum. M. K. E. Husein. S. Permana. A. Rustandi. and J. W. Soedarsono. "A preliminary study on the reduction of limonite ore by using rice husk as a reducing agent." *IOP Conf. Ser. Mater. Sci. Eng.*. vol. 316. no. 1. p. 012050. 2018.
17. M. F. Ghiyats. A. Maksum. and J. W. Soedarsono. "Preliminary study on the use of rice husk as a reducing agent in iron sand reduction." *IOP Conf. Ser. Mater. Sci. Eng.*. vol. 553. no. 1. 2019.

18. H. T. B. M. Petrus. A. D. P. Putera. E. Sugiarto. I. Perdana. I. W. Warmada. F. Nurjaman. W. Astuti. and A. T. Mursito. "Kinetics on roasting reduction of limonitic laterite ore using coconut- charcoal and anthracite reductants." *Miner. Eng.*. vol. 132. no. 2. pp. 126–133. 2019.
19. D. Nayak. N. Dash. N. Ray. and S. S. Rath. "Utilization of waste coconut shells in the reduction roasting of overburden from iron ore mines." *Powder Technol.*. vol. 353. pp. 450–458. 2019.
20. J. W. Soedarsono. C. E. Arifin. J. S. Saragi. A. A. Putra. A. Kawigraha. R. D. Sulamet-Ariobimo. and A. Rustandi. "The Effect of Reduction Parameter in Processing Lump Ore with Green Sugarcane Bagasse Reductor in Muffle Furnace." *Mater. Sci. Forum*. vol. 893. pp. 195–201. 2017.
21. PT Vale Indonesia and Tbk. "PT Vale Indonesia Process Plant Introduction." 2017.
22. K. N. Chethan. L. G. Keni. N. H. Padmaraj. A. Dias. and R. Jain. "Fabrication and Mechanical characterization of aluminium [6061] with conventionally prepared bamboocharcoal." *Mater. Today Proc.*. vol. 5. no. 2. pp. 3465–3475. 2018.
23. S. S. Tsalidis. A. J. Dentsoras. and P. Maresca. "Application of design parameters space search for belt conveyor design." *Eng. Appl. Artif. Intell.*. vol. 10. no. 6. pp. 617–629. 1997.

RiESTech
Recent in Engineering Science and Technology

MBI

Article

Application of an Automated System for Converting Waste Cooking Oil into Aromatherapy Candles

Hasvienda M Ridlwan[1,*], Ahmad Adifani[1] and Vernida Mufida[2]

[1] Department of Mechanical Engineering, Politeknik Negeri Jakarta, Depok 16425, Indonesia
[2] PT Badak NGL, Bontang, Kalimantan Timur, 75324
* Correspondence: hasvienda.ridlwan@mesin.pnj.ac.id

Abstract: This research focuses on the development of an automated system for the production of aromatherapy candles using waste cooking oil. The study addresses the challenges faced in small-scale production, including limited capacity, manual processes, and inconsistent product quality. To overcome these challenges, an automated machine is proposed to improve efficiency and productivity. The homogenization process and heating time were identified as critical areas for improvement. A sequential control system was successfully implemented, enabling the conversion of waste cooking oil into aromatherapy candles with a production capacity of 10.5 liters per unit run. The motor control system utilized On-Off control with modified power input to minimize vibration issues, operating the motor at 50-60 RPM. The temperature heater control system employed a PID control method, specifically the Ziegler-Nichols type 2 method, with Kp and Ki values of 247.5 and 1.104, respectively. The chosen PID parameters demonstrated satisfactory perfor-mance, including a rise time of 22.95 minutes, maximum overshoot of 2.85%, and a dead time of 510 seconds. The implemented system was controlled using an Arduino controller, ensuring a fast response and stable operation.

Keywords: Automation; Aromatherapy Candle Machine; PID; Control; Arduino.

Citation: M Ridlwan, H., Adifani, A., & Mufida, V. (2023). Application of an Automated System for Converting Waste Cooking Oil into Aromatherapy Candles. Recent in Engineering Science and Technology, 1(03). https://doi.org/10.59511/riestech.v1i03.20

Academic Editor: Iwan Susanto

Received: 12 May 2023
Accepted: 29 May 2023
Published: 1 July 2023

Publisher's Note: MBI stays neutral with regard to jurisdictional claims in published maps and institutional affiliations.

1. Introduction

In general, the Indonesian population has a preference for fried foods. This has led to an increasing consumption of palm oil for cooking purposes each year, parallel to the population growth. Based on data from the Indonesian Central Bureau of Statistics (BPS) in 2019, the per capita consumption of palm oil for cooking purposes reached 10.79 liters per year in 2018. It is predicted that the consumption of palm oil for cooking purposes in 2019 and 2020 will increase to approximately 11.09 and 11.38 liters per capita per year, respectively[1].

The household economy exhibits significant diversity, resulting in varying practices regarding the usage of cooking oil. While some households dispose of cooking oil after a single use, others employ it for multiple frying sessions. Typically, cooking oil can be safely used for up to 3 or 4 frying sessions. However, when cooking oil is repeatedly reused, its fatty acid content becomes more saturated, causing a color change known as "used cooking oil" or "minyak jelantah." This used cooking oil is highly unsuitable for consumption or further reuse in frying food. The continuous ingestion of used cooking oil and its subsequent accumulation in the human body can lead to long-term health issues. Negative consequences of consuming used cooking oil include abnormal fat deposits, an increased risk of cancer, and the loss of neural control functions[1, 2].

Used cooking oil waste is a prevalent problem in the culinary sector, from large restaurants to street vendors and households. Cooking food typically involves frying, leading to the production of used cooking oil waste in every household[1].

Used cooking oil is a waste product generated from the consumption of cooking oil, both in household settings, restaurants, street vendors, and other needs. In the Badak LNG environment, there is used cooking oil waste generated by Badak LNG's partner, such as catering services. The amount of waste generated by the catering services of PT Badak NGL's partners is quite significant, ranging from twenty-five to fifty liters per week. This is consistent with the high demand for food orders almost every day. If not properly managed, the generated used cooking oil waste can pollute the environment when disposed of in sewers, ditches, soil, and other areas. It is essential to implement effective waste management to ensure environmental sustainability. There are various options for treating used cooking oil waste to avoid wasteful disposal, As previously conducted by researchers, there have been various approaches to address the issue like Processing of used cooking oil (jelantah) as a substitute for kerosene fuel (biofuel)[3], Conversion of used cooking oil waste into dishwashing soap for pollution mitigation and community empowerment[4], Utilization of leftover cooking oil waste and coffee grounds to produce scented soap for household use and as an alternative for small-scale household industries[5, 6].

The partner of PT Badak LNG, through Salin Swara (Sampah Keliling Swadaya Masyarakat), has conducted experiments on small-scale production of aromatherapy candles utilizing used cooking oil waste. However, several challenges were encountered during the experiment, including limited production capacity, manual heating and stirring processes, and inconsistent product quality. To address these challenges, a dedicated unit is required to process the used cooking oil waste into aromatherapy candles, enabling Salin Swara to produce them more easily and effectively. Through this research, an automated machine is proposed to expedite the process by transforming manual tasks into automated ones, aiming to enhance efficiency and productivity. In the small-scale production conducted at the laboratory level, several challenges were encountered during the process of making aromatherapy candles. One of the challenges was the inadequate quality of the resulting aromatherapy candles due to an ineffective homogenization process. Additionally, the heating process for the mixture took a long time. Furthermore, the process of converting used cooking oil waste into aromatherapy candles was lengthy, highlighting the need for an automated system to facilitate the production process.

Therefore, this research focuses on addressing these challenges by designing an automated system for the processing unit of used cooking oil waste into aromatherapy candles. The aim is to enable the production of aromatherapy candles to be conducted more easily and effectively. The automation system is designed to allow users to perform the production process of aromatherapy candles with ease, safety, and efficiency. The automation system includes motor control for stirring, heating elements, valves, pumps, and their sequential operations. The expected outcome of this research is to efficiently and effectively process used cooking oil waste into high-quality aromatherapy candles.

2. Materials and Experiment Methods

The process flow of converting used cooking oil waste into aromatherapy candles like Figure 1 is as follows:

a) The used cooking oil waste enters an adsorption and filtration column for the process of filtering and absorbing impurities present in the waste. This absorption process involves the use of specially treated bananas.
b) The used cooking oil waste is pumped into a feed storage before being used as a raw material for the production of aromatherapy candles.
c) A manual valve at the bottom of the feed storage is used for sampling and draining the used cooking oil waste.

d) If the used cooking oil waste that has passed through the adsorption and filtration column does not meet the required quality standards, it undergoes another round of adsorption and filtration process until the desired results are achieved.
e) The compliant feed oil is pumped into a mixer column.
f) Stearic acid, in powder form, is introduced into the mixer column using a modified valve with the assistance of a servo.
g) Liquid dye is introduced into the mixer column through gravity flow, with the solenoid valve opening and closing based on a predetermined time delay.
h) Fragrance is introduced into the mixer column through gravity flow by opening the solenoid valve located below. The solenoid valve opens based on a predetermined time delay.
i) The mixer and heater are activated according to the established operational specifications.
j) The resulting aromatherapy candle product is collected in prepared containers.

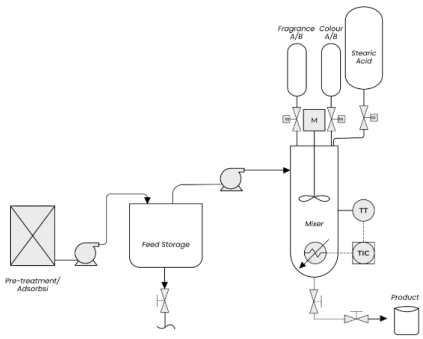

Figure 1. Process and Flow Diagram

The control system of the aromatherapy candle production unit utilizes sequential control, which is regulated by an Arduino Mega. The steps of the control system align with the explanations provided in the Process and Flow Diagram (PFD). The Arduino Uno is specifically used for controlling the motor and heater. The Arduino Mega acts as the main controller, overseeing the sequential control of the entire process. It receives input signals from various sensors and switches, enabling it to monitor the status of the process and trigger the necessary actions. The Arduino Uno is dedicated to controlling the motor and heater. It receives commands from the Arduino Mega and executes the corresponding actions can see at Figure 2 and Figure 3 for protection line for machine. For example, it controls the motor's speed and direction for the mixer column, as well as the heater's temperature for the heating process. By integrating these Arduino boards into the control system, precise and automated control of the production process of aromatherapy candles can be achieved, ensuring consistent quality and efficient operation.

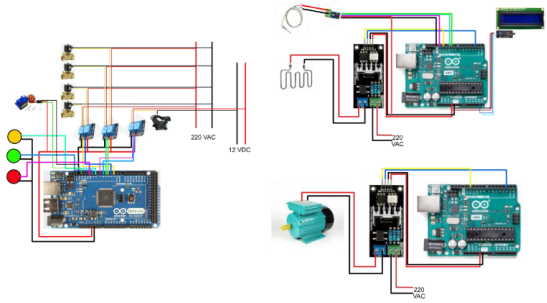

Figure 2. Schematic of automatic control machine

The pump in the aromatherapy candle production unit is powered by a 12V motor voltage. The pump's primary function is to circulate the liquid fluid, which is the feed used cooking oil. Additionally, the pump is responsible for transferring the treated used cooking oil to the feed storage column.

The pump that transfers the used cooking oil to the feed storage column is controlled using a simple on-off mechanism, without the use of a relay. On the other hand, the pump that transfers the used cooking oil into the mixer column utilizes a relay, which remains active for a predetermined time delay.

The servo functions as a valve for the stearic acid. It operates as a driving mechanism to open and close the pipe for a specific period based on the obtained time delay. The servo changes its position from 0 degrees to 180 degrees when it is open. Once the time delay is reached, the servo returns to its previous position.

The Solenoid Valve operates in an on-off mode based on the predetermined sequential or alternate process flow. It is controlled using a relay for its operation.

The Heater functions as the heating element for the entire material. It is controlled using a PID (Proportional-Integral-Derivative) controller with the assistance of a Zero Cross AC Light Dimmer. A K-type thermocouple sensor[7] is employed to provide real-time temperature readings at intervals of 500 ms.

The Motor's output voltage is regulated using a Zero Cross AC Light Dimmer[8, 9]. The voltage is adjusted to maintain a constant RPM (Revolutions Per Minute) as per the predetermined parameters.

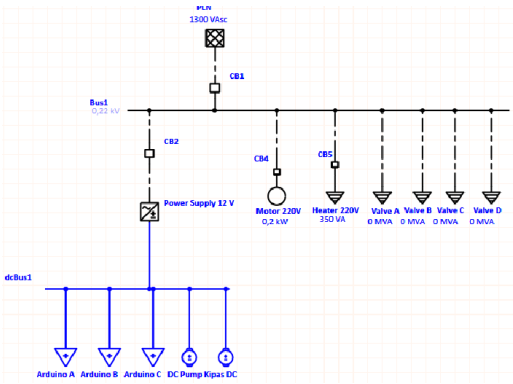

Figure 3. Schematic of automatic control machine

Tuning is the term used to describe the methods used to select the optimal control settings to achieve a specific performance outcome. In this research, two tuning methods are used for PID tuning, namely the Ziegler-Nichols type 2 method and the Cohen-Coon method. The Ziegler-Nichols type 2 method is a widely used tuning method that involves identifying the critical gain and critical period of the system. Based on these values, the proportional, integral, and derivative gains of the PID controller are calculated. The Cohen-Coon method is another tuning method that focuses on determining the ultimate gain and ultimate period of the system. These values are then used to calculate the PID gains. Both methods aim to find the optimal PID controller parameters that provide stable and satisfactory performance for the heating process in the research. The choice of which method to use depends on factors such as the system dynamics and the desired performance criteria[10]. The Ziegler-Nichols type 2 method disregards the integral and derivative actions of the PID controller and focuses only on the proportional gain, Kp. The value of Kp is gradually increased from a low value until the system exhibits sustained oscillations without any clear increase or decrease. The value of Kp that produces this response is then recorded as Kcr (critical gain). Once Kcr is determined, the Ziegler-Nichols type 2 method provides formulas to calculate the optimal PID values based on Kcr. These formulas involve adjusting the proportional, integral, and derivative terms using predetermined factors. The Ziegler-Nichols type 2 method is a commonly used technique for tuning PID controllers to find optimal control parameters.

Although this method is relatively simple, it can provide satisfactory results for stable systems with clear oscillations.

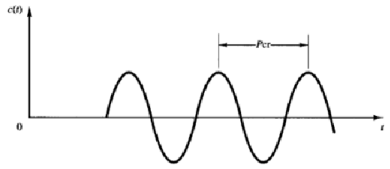

Figure 4. Determine Pcr Parameter response

The PID tuning method of Ziegler-Nichols type 2 recommends adjusting the PID parameters based on the obtained values of Kcr and Pcr. The recommended tuning values are as follows:

Table 1. Parameter of Ziegler-Nichols 2

Mode	**K_p**	**T_i**	**T_d**
P	0.5*Kcr	-	-
PI	0.45*Kcr	0.85*Pcr	-
PID	0.6*Kcr	0.5*Pcr	0.12*Pcr

In Table 1, Kp, Ti, and Td represent the proportional gain, integral time, and derivative time values, respectively. The P mode uses only proportional control, the PI mode uses proportional and integral control, and the PID mode uses proportional, integral, and derivative control. By using Table 1, you can adjust the PID values according to the desired response of your system. Please note that the Ziegler-Nichols method is a general tuning method and may need further adjustments depending on the characteristics of your specific system.

The Cohen-Coon method is typically used for open-loop systems. The Cohen-Coon tuning rules are suitable for self-regulating processes when the control objective requires a fast response. It is recommended to divide the calculated controller gain by two. The Cohen-Coon method is particularly suitable for systems with a significant dead time. In the Cohen-Coon method, the process is conducted by applying a step input to the open-loop system until the response reaches a steady state. Once the response reaches a steady state, another step input is applied. The resulting signal of the change is used to design the PID values. By analyzing the response to the second step input, specific parameters can be determined to calculate the PID values. These parameters include the ultimate gain (Ku), ultimate period (Pu), and ultimate time (Tu). The ultimate gain is the maximum change in output divided by the change in input during the second step response.

3. Results And Discussion

The Mixer Column at Figure 5 serves as the location for the homogenization (mixing) of all the ingredients used in aromatherapy candle production, including 3 L of used cooking oil, 7 kg of stearic acid, 400 mL of fragrance, and 100 mL of colorant. The homogenization process takes approximately 45 minutes to 1 hour at a setpoint temperature of around 70 degrees Celsius. The Heater is used to heat the Mixer Column and is controlled by a PID controller to maintain the desired temperature effectively.

The Motor is utilized to drive the agitator, which facilitates the mixing of the used cooking oil, stearic acid, fragrance, and colorant. Based on laboratory-scale experiments, it was found that the ingredients do not mix evenly without agitation. However, excessive agitation can lead to the formation of foam. Therefore, a gentle agitation technique is required to ensure thorough mixing of all the ingredients without excessive foaming.

Figure 5. Automtic Machine for Converting Waste Cooking Oil into Aromatherapy Candles

In this research, a 350 Watt heater at Figure 6 and a 200 Watt motor are utilized. The heater is controlled using a PID controller with the assistance of a Zero Cross AC Light Dimmer PWM. The PID control ensures effective temperature regulation at the setpoint. The 200 Watt motor, when used as the agitator at a temperature of 70 degrees Celsius, is found to be too powerful. Therefore, voltage control is implemented for the motor, specifically set at 40 V. Through testing, it has been determined that at this voltage, the motor can rotate at a speed ranging from 50 to 60 RPM. This voltage control approach allows achieving the desired mixing intensity without excessive agitation.

Figure 6. Heater element

3.1. Control Technique

3.1.1. Sequential Control System

Sequential Control System is a control system that performs a series of control operations in a predetermined sequence. Typically, sequential control executes commands that have two states sequentially, such as start/stop, up/down, close/open, on/off signals, and so on. The system follows a predefined order of operations to achieve the desired control objectives. Sequential control is commonly used in various applications where specific actions need to be carried out in a specific order or sequence.

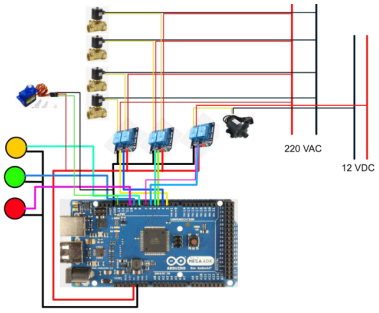

Figure 7. Arduino Mega for sequential controlling valve and servo

Figure 7 describe the sequential control system used to regulate the sequence of the aromatherapy candle production process using waste cooking oil as the main ingredient in an automated system consists of several components.

3.1.2 The control system for the mixer motor

In the homogenization process of the ingredients for aromatherapy candle production in the mixer column, thorough mixing of the ingredients is necessary to ensure proper composition. The mixing is achieved using an agitator powered by an AC motor. The AC motor is controlled by an Arduino Uno R3 through a zero-cross AC dimmer. The motor is controlled using On-Off control with additional power manipulation modifications. Power manipulation is implemented to address the issue of vibration when the agitator receives full power from the AC motor. Therefore, tests were conducted to determine the appropriate power level for the AC motor like Figure 8 as the driver for the agitator.

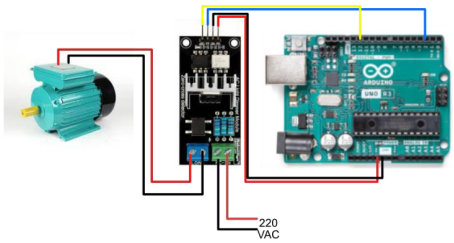

Figure 8. Arduino and AC dimmer controlling the mixer motor

The AC electric motor at Figure 9 is an electromechanical device that converts electrical energy into mechanical energy. It consists of two main components: the stator (stationary part) and the rotor (rotating part). When electric current flows through the stator, magnetic field lines or flux lines are generated, resulting in the production of an electromagnetic force (EMF) that creates a rotating field, following Faraday's Law. The AC motor serves as the driving mechanism for the agitator in the mixer column, which has been designed by the mechanical team. However, the agitator has a limitation due to poor installation of the coupling/connection between the motor and the agitator. Visually, it can be observed that the alignment of the shaft connection is not optimal. As a result, when rotational power is applied from the selected AC motor, significant vibrations occur. These vibrations cause the upper support section to shake and result in the agitator colliding with the walls of the mixer column. To address this issue, power input control is implemented for the AC motor. After conducting tests, the agitator operates at an RPM of 50-60 to mitigate the vibrations and maintain stable operation.

Figure 9. Single Phase AC Motor

3.1.3 Temperature control system

In the process of homogenizing the ingredients for making aromatherapy candles in the mixer column, a heating system is necessary to ensure proper mixing of all the materials. The stearic acid needs to be heated to melt and blend with the other ingredients. The heater is designed to operate above the melting point of stearic acid and below the boiling point of the used cooking oil. A set point temperature of 70 degrees Celsius has been determined for the heater control. The control system is designed to rapidly reach the target temperature of 70 degrees Celsius and maintain it effectively.

The temperature of the heater with Arduino uno and dimmer at Figure 10 is controlled using a PID (Proportional-Integral-Derivative) control scheme, specifically em-

ploying the PI (Proportional-Integral) mode. This choice is made to ensure the system exhibits a fast response time to reach the set point temperature and minimizes steady-state error.

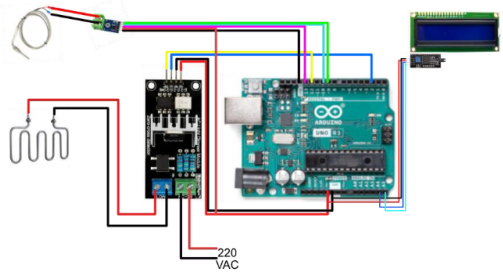

Figure 10. Arduino Uno and Dimmer Controlling Temperature

3.2. Experimantal Testing

3.2.1 DC pump 12V

Testing of the DC 12 V pump component was conducted by supplying electrical current to the pump, allowing it to circulate used cooking oil. The circulated oil was collected in a designated container. The volume of the circulated used cooking oil was measured and compared with the pump's operating time can see at eq 1.

$$Q = V/t, \tag{1}$$

Q = Discharge
V = Volume
t = Time

3.2.2 Thermocouple type K

Testing of the Type K thermocouple was conducted using a sampling method and comparing the measurement data with a reference thermometer. Data was collected within a temperature range of 30 to 100 degrees Celsius can see data at Table 2. Sampling was recorded for every 5-degree Celsius increment on the thermometer.

Table 2. Experimental Testing Thermometer beetwen Type K Thermocouple

	Sensor read	**Error (°c)**
Thermometer	Type K thermocouple	
30	30	0
35	34,75	0,25
40	39,5	0,5
45	45	0
50	49,25	0,75
60	60,25	0,25
65	65	0
70	69,75	0,25
75	74,5	0,5
80	79,5	0,5
85	85	0
90	90,25	0,25
95	94,75	0,25
100	100,25	0,25

3.2.3 Agrigator motor and Zero Cross Detector

Testing of the motor and Zero Cross was conducted to understand the behavior of the motor and Zero Cross based on input from the Arduino. The Zero Cross controls the Z-C signal provided by the Arduino (0-1024) and represents it as a percentage from 0 to 100%. The table above represents direct measurements taken when the motor acted as the agitator drive and was supplied with different voltage variations. The motor started moving when a voltage of 33 V was applied can see data experimental at Table 3.

Table 3. Experimental Testing Motor Speed

Speed (%)	(1-1024)	Voltage (V)	RPM
5	51,2	3	0
10	102,4	8	0
15	153,6	13	0
20	204,8	22	0
25	256	33	22
30	307,2	45	100
35	358,4	61	148
40	409,6	80	166
45	460,8	95	180
50	512	112	>180
55	563,2	132	>180
60	614,4	148	>180
65	665,6	164	>180
70	716,8	174	>180
75	768	190	>180
80	819,2	201	>180
85	870,4	212	>180
90	921,6	217	>180
95	972,8	220	>180
100	1024	220	>180

At Figure 11 voltages above 95 V, the agitator motor will rotate at a speed of 180 RPM. At this RPM, the upper support of the mixer column will vibrate, and the motor becomes unstable, causing the agitator to collide with the walls of the mixer column. If the voltage supplied to the motor exceeds 95 V, it is certain that the agitator motor is outside the specifications of the mixer column. In this case, a voltage of approximately 40 V is chosen as the appropriate voltage that aligns with the mixer's specifications and the aromatherapy candle manufacturing process.

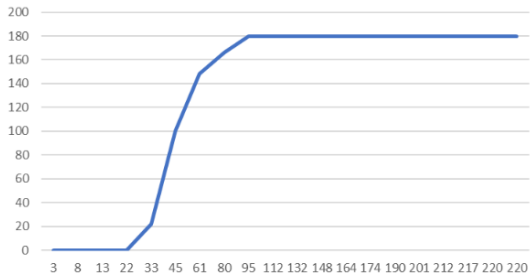

Figure 11. Graphic of experimental motor

3.3 PID Tunning

Tuning refers to the methods used to select the optimal control settings to achieve a specific performance. There are two methods used in PID tuning in this paper, the Ziegler-Nichols type 2 method and the Cohen-Coon method.

3.3.1 Tunning Ziegler-Nichols type 2 method

In this case, the integral and derivative actions are disregarded. The system is only given the proportional gain (Kp) value. The Kp value is gradually increased from the

lowest value until the system exhibits sustained oscillation without any noticeable increase or decrease. The Kp value that produces this response is then recorded and referred to as Kcr. The Pcr value is obtained from the time between two peaks in the system's response.

From Figure 12 , the value of Kcr is 550 and the value of Pcr is 269. Based on these values.

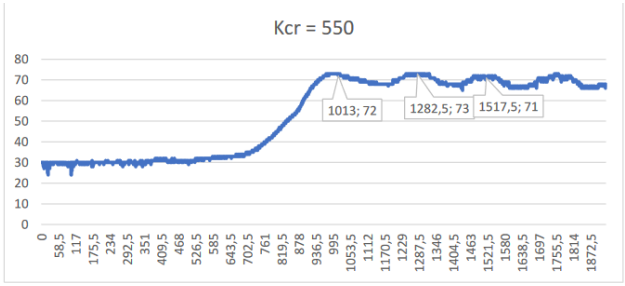

Figure 12. Oscilation of heater

In this paper, a PI controller was chosen because it requires a fast response and is able to maintain steady-state conditions. The system response tends to be smooth, and sustained oscillations were only observed at the Kcr value of 550. Therefore, the decision was made to only use the PI controller without incorporating the derivative control.

Determine Kp and Ki Value from equations 2 and 3.

$$Kp = 0{,}45 \times Kcr \tag{2}$$

$$Kp = 0{,}45 \times 550 = 247{,}5$$

$$Ti = \frac{1}{1{,}2} \times Pcr \tag{3}$$

$$Ti = \frac{1}{1{,}2} \times 269 = 224{,}16$$

$$Ki = \frac{Kp}{Ti}$$

$$Ki = \frac{Kp}{Ti} = \frac{247{,}5}{224{,}16} = 1{,}104$$

3.3.2 Ziegler-Nichols type 2 Response analsys

Figure 13 represents the data obtained from the overall heating process of the materials used in aromatherapy candle production by the temperature heater control system. Based on the graph, the control system has a rise time of 1377.5 seconds or 22.95 minutes, a maximum overshoot at a temperature of 72 degrees Celsius or 2.85% of the set point, and a dead time of 510 seconds.

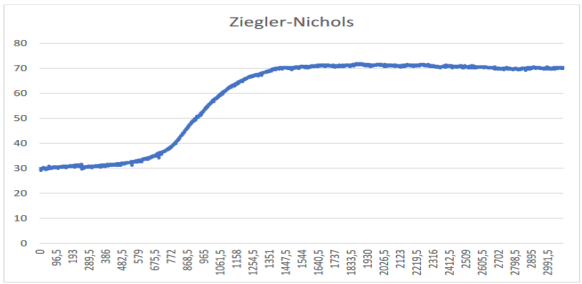

Figure 13. Graphic Ziegler-Nichols type 2 Heater response analsys

3.3.3 Tunning Cohen-Coon method

The Cohen-Coon method is typically used for open-loop systems. The Cohen-Coon tuning rules are suitable for self-regulating processes where the control objective requires a fast response, but it is recommended to divide the calculated controller gains by two. The Cohen-Coon method is suitable for systems with a significant dead time. This method is performed by applying a step input to the open-loop system until the response reaches a steady-state. After reaching the steady-state, another step input is applied to the system. The resulting signal of the change is then used to design the PID values.

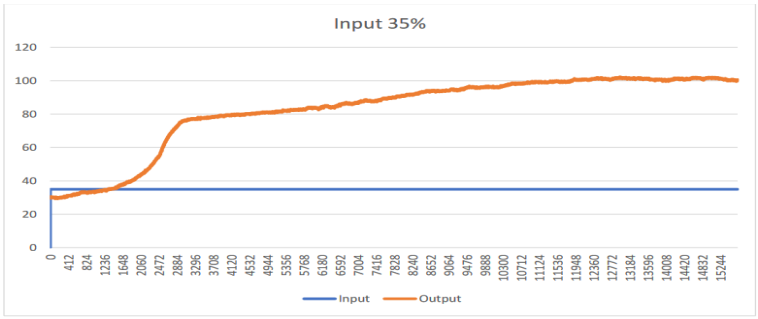

Figure 14. Graphic Cohen-Coon Heater response analsys

Figure 14 represents the data obtained from the overall heating process of the materials used in aromatherapy candle production by the temperature heater control system with input step power 35%, Dead time (td) is 977 s.

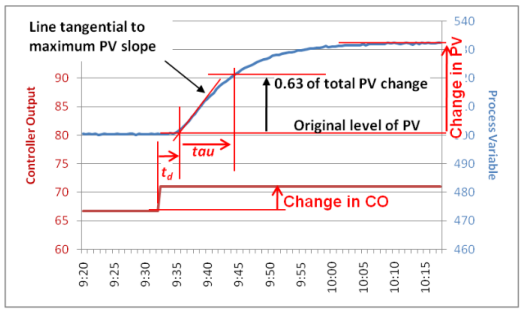

Figure 15. Graphic Slope Heater response analsys

From Figure 15 we can determine:

Change in PV = 102 – 29 =73, Change in CO = 35 – 0 = 35, 0,632 * change in pv = 46,136, tau (t) = 1197,5, gp = change in PV/change in CO = 73/35 = 2,085714.

Determine Kc and Ki Value from equations 4 and 5.

$$Kc = \frac{0,9}{Gp}\left(\frac{t}{td} + 0,092\right) \quad (4)$$

$$Kc = \frac{0,9}{2,085714}\left(\frac{1197,5}{977} + 0,092\right) = 0,5685$$

$$Ti = 3,33td\,\frac{t + 0,092\ td}{t + 2,22\ td} \quad (5)$$

$$Ti = 3,33(977)\frac{1197,5 + 0,092\ (977)}{1197,5 + 2,22\ (977)}$$

$$Ti = 1244,159$$

$$Ki = \frac{Kc}{Ti} = \frac{0,5685}{1244,159} = 0,000457$$

3.3.4 Cohen-Coon response analysis

Figure 16 represents the data obtained from the overall heating process of the ingredients in aromatherapy candle production by the temperature heater control system. Based on the graph, the control system has a rise time of 4835 seconds or 80.58 minutes, a maximum overshoot at a temperature of 70.5 degrees Celsius or 0.714% of the set point, and a dead time of 1746 seconds.

4. Conclusions

In conclusion, the application of an automatic system with sequential control was successfully implemented in the processing unit of converting waste cooking oil into aromatherapy candles with a production capacity of 10.5 liters per unit run. The motor control system for the agitator was implemented using an On-Off control with power input modification to mitigate vibration issues. The motor was controlled to operate at a speed of 50-60 RPM. The temperature heater control system was implemented using a PID control method.

For the PID tuning, the Ziegler-Nichols type 2 method was chosen, resulting in a Kp value of 247.5 and Ki value of 1.104. This tuning configuration provided satisfactory performance with a rise time of 22.95 minutes, maximum overshoot of 2.85%, and a dead time of 510 seconds. The chosen PID parameters ensured a fast response and maintained stable conditions.

Overall, the implemented automatic system with sequential control, motor control, and temperature heater control proved to be effective in the production process of aromatherapy candles from waste cooking oil. The selected PID tuning parameters based on the Ziegler-Nichols method demonstrated good performance characteristics, contributing to efficient and reliable operation.

Acknowledgments: I am sincerely grateful to Ahmad Adifani and Vernida Mufida for his continuous support and assistance in this research. I would also like to express my heartfelt gratitude to PT Badak NGL academy for their valuable collaboration with PNJ research and teamwork.

References

1. F. Damayanti and T. J. D. J. P. K. M. Supriyatin, "Pemanfaatan limbah minyak jelantah sebagai upaya peningkatan kepedulian masyarakat terhadap lingkungan," vol. 5, no. 1, 2021.
2. E. Lotero *et al.*, "Synthesis of biodiesel via acid catalysis," vol. 44, no. 14, pp. 5353-5363, 2005.
3. N. E. Setyaningsih and W. S. J. R. J. P. T. d. P. Wiwit, "Pengolahan minyak goreng bekas (jelantah) sebagai pengganti bahan bakar minyak tanah (biofuel) bagi pedagang gorengan di sekitar fmipaunnes," vol. 15, no. 2, pp. 89-95, 2018.
4. R. D. Kusumaningtyas, N. Qudus, R. D. A. Putri, and R. J. J. A. Kusumawardani, "Penerapan teknologi pengolahan limbah minyak goreng bekas menjadi sabun cuci piring untuk pengendalian pencemaran dan pemberdayaan masyarakat," vol. 22, no. 2, pp. 201-208, 2018.
5. L. Roza and W. D. J. P. S. Laksanawati, "Pemanfaatan limbah sisa minyak goreng dan serbuk kopi menjadi sabun wangi untuk keperluan rumah tangga dan alternatif industri skala rumah tangga sebagai konsep mandiri ekonomi bagi anggota koperasi wanita flamboyan Ciracas Jakarta Timur," vol. 1, pp. 247-250, 2018.
6. L. Suryani, A. U. Aje, and K. J. D. J. P. K. M. j Tute, "PKM pelatihan kelompok anak cinta lingkungan Kabupaten Ende dalam pegelolaan limbah organik dan anorganik berbasis 3R untuk mengeskalasi nilai ekonomis barang sebagai bekal wirausaha mandiri," vol. 3, no. 2, pp. 244-251, 2019.
7. N. Evalina, F. I. Pasaribu, A. Azis, and A. J. R. J. T. E. Sary, "Penggunaan Arduino Uno Untuk Mengatur Temperatur Pada Oven," vol. 4, no. 2, pp. 122-128, 2022.

8. A. G. Ekayana and A. A. R. J. J. P. T. D. K. Rakasiwi, "Rancang Bangun Pengaman Power Supplay Berbasis Zero Crossing Detector Pada Laboratorium Komputer," vol. 15, no. 1, 2018.
9. V. Venny, E. Setyaningsih, and Y. J. T. J. T. E. Calvinus, "Perancangan Dan Realisasi Automatic Dimming Light Pada Laboratorium Pendidikan," vol. 24, no. 1, pp. 82-90, 2022.
10. M. D. I. Putri, A. Ma'arif, and R. D. J. T. Puriyanto, "Pengendali Kecepatan Sudut Motor DC Menggunakan Kontrol PID dan Tuning Ziegler Nichols," vol. 23, no. 1, pp. 9-18, 2022.

RiESTech
Recent in Engineering Science and Technology

MBI

Article

Machine Failure Detection using Deep Learning

Idrus Assagaf [1,*], Agus Sukandi [1], Abdul Azis Abdillah [2]

[1] Department of Mechanical Engineering, Politeknik Negeri Jakarta, Depok 16425, Indonesia
[2] Department of Mechanical Engineering, University of Birmingham, Birmingham, United Kingdom
* Correspondence: idrus.assagaf@mesin.pnj.ac.id

Abstract: This article focuses on the application of deep learning methods for failure prediction. Failure prediction plays a crucial role in various industries to prevent unexpected equipment failures, minimize downtime, and improve maintenance strategies. Deep learning techniques, known for their ability to capture complex patterns and dependencies in data, are explored in this study. The research employs Multi-Layer Perceptron as deep learning architectures. This model is trained on AI4I 2020 Predictive Maintenance data to develop accurate failure prediction models. Data preprocessing involves cleaning, feature engineering, and normalization to ensure the quality and suitability of the data for deep learning models. The dataset is split into training and testing sets for model development and evaluation. Performance evaluation metrics such as accuracy, ROC, and AUC are utilized to assess the models' effectiveness in predicting failures. The experimental results demonstrate the effectiveness of deep learning methods in failure prediction. The models showcase high accuracy and outperform SVM approaches, particularly in capturing intricate patterns and temporal dependencies within the data. The utilization of Multi-Layer Perceptron architecture further enhances the models' ability to capture long-term dependencies. However, challenges such as the availability of diverse and high-quality data, the selection of appropriate architecture and hyperparameters, and the interpretability of deep learning models remain sig-nificant considerations. Interpretability remains a challenge due to the inherent complexity and black-box nature of deep learning models. In conclusion, deep learning method offer significant potential for accurate failure prediction. Their ability to capture complex patterns and temporal dependencies makes them well-suited for analyzing operational and sensor data. Future research should focus on addressing challenges related to data quality, interpretability, and model opti-mization to further enhance the application of deep learning in failure prediction.

Keywords: Failure prediction; Deep learning; Multi-Layer Perceptron

Citation: Assagaf, I., Sukandi, A., & Abdillah, A. A. (2023). Machine Failure Detection using Deep Learning. Recent in Engineering Science and Technology, 1(03), 26–31. https://doi.org/10.59511/riestech.v1i03.21

Academic Editor: Iwan Susanto

Received: 24 May 2023
Accepted: 12 June 2023
Published: 1 July 2023

Publisher's Note: MBI stays neutral with regard to jurisdictional claims in published maps and institutional affiliations.

1. Introduction

In today's industry, efficient and timely maintenance of production equipment is essential to maintain smooth operations and avoid unforeseen breakdowns. Traditionally, maintenance is carried out routinely based on a predetermined schedule or based on visible signs of damage. This approach is often ineffective as overly frequent maintenance can lead to high maintenance costs, while late or improper maintenance can cause severe equipment damage and disrupt production [1].

In the last few decades, technological developments have opened up new opportunities in equipment maintenance through a predictive maintenance approach. Predictive maintenance [2] is an approach that continuously monitors equipment conditions using sensors and related technologies. By analyzing the data generated by the sensor, be it vibration, temperature, pressure, or other parameters, and leveraging machine learning techniques, we can identify the early signs and patterns that lead to equipment failure. This way, we can take the necessary precautions before significant damage occurs.

Research on predictive maintenance using machine learning has become popular in the industry in recent years. Li et al. [3] built failure prediction models to avoid service interruptions and increase rail network velocity. By using SVM to build a predictive model for railway maintenance, the experimental results obtained show that the model built can significantly increase business value. Kanawaday et al. [4] used the AutoRegressive Integrated Moving Average (ARIMA) statistical method to predict the probability of machine failure and production defects resulting from machine slitting, where data is collected through several sensors installed in the engine. The results indicate that the predictive maintenance model can reduce maintenance costs and improve the quality of the manufacturing process.

Amruthnath et al. [5] implemented unsupervised learning to perform early failure detection on submachines. The data used is vibration data originating from an exhaust fan. Of the several methods used, such as Principle Component Analysis (PCA) T2 statistics, Hierarchical clustering, K-Means clustering, C-Means, and Model-based clustering, T2 statistics can outperform other methods in detecting early failures. Gohel et al. [6] proposed using machine learning such as Support Vector Machine (SVM) and Logistic Regression to perform predictive maintenance on nuclear infrastructure.

Sharma et al. [7] conducted a comparative study using machine learning to predict machine failure based on several predictive maintenance datasets. The datasets used include Ai4i2020 Predictive Maintenance Dataset, MZVAV-2-1 Dataset, CWRU - Bearing Modified Dataset and Electrical power transmission fault dataset. The random forest method can outperform other machine learning methods such as SVM, Decision Tree, KNN, and Logistic Regression.

From this literature review, predictive maintenance using machine learning has become a promising research area in increasing the efficiency of equipment maintenance. This approach leverages sensor data and machine learning techniques to identify early signs of failure, so companies can take the necessary countermeasures before significant damage occurs. Previous research has succeeded in developing an accurate damage prediction model using SVM, Arima, Logistic Regression, regression algorithms, and the other machine learning models.

However, despite significant progress in this area, there is still room for further development. In this research, we will take advantage of the experience from previous studies and go a step further by developing a failure prediction model using deep learning techniques based on multi-layer perceptron architecture. Combining sensor data, maintenance logs, and historical breakdown data, we aim to create a more accurate and reliable model for implementing a predictive maintenance approach in the manufacturing industry.

The main objective of this research is to develop a failure prediction model using a multi-layer perceptron technique to implement a predictive maintenance approach. Using data collected in real time, this model will be trained to recognize critical patterns that may indicate equipment damage or failure. Thus, the company can perform maintenance based on the actual condition of the equipment, avoid unnecessary maintenance, and optimize the use of resources.

2. Materials and Experiment Methods

The research methodology consists of ten main steps. First, the problem to be studied in the predictive maintenance domain is identified, focusing on machine failure prediction. The research aims to develop an accurate predictive model to support predictive maintenance. The second step involves collecting dataset. Dataset used in this experiment is AI4I 2020 Predictive Maintenance data [8-10]. After that, third stage, the collected data is processed and cleaned, including missing values, outliers, and noise handling. Explorative data analysis was carried out as the next step, aiming to understand the characteristics, patterns, and relationships between variables.

After that, fourth stage, the prediction model was developed using the Multi-layer Perceptron deep learning method. The model is trained using processed data. The model parameters were adjusted, and cross-validation was performed to improve the performance and generalization of the model.

Finally, model evaluation is performed using appropriate evaluation metrics, such as accuracy, ROC, and area under the ROC curve, to measure model performance. The model is evaluated using the validation data to test the model's predictive ability on data that has never been seen before. If necessary, optimization and tuning of model parameters are performed to improve predictive performance. By following this methodology, it is expected to develop accurate and relevant predictive models to support predictive maintenance efforts in the predictive maintenance domain.

3. Results and Discussion

a. Machine Failure Dataset

This study used the AI4I 2020 Predictive Maintenance Dataset [8-10] in an experiment using a Multi-Layer Perceptron (MLP). This dataset has several variables that are used to determine the failure of a machine. These variables include product ID, Ambient Temperature, Process Temperature, Rotation velocity, torque, and wear and tear. This data shows an unequal proportion between failed and normal machine behaviour labels, where the percentages are 4% and 96%, respectively. In the early stages of the experiment, the dataset was undersampled and normalized before entering the modelling stage. In this experiment, the proportion of training and testing data for training was divided into the first three compositions 90%: 10%, the second 80%: 20% and the last 70%: 30%.

b. Performance evaluation

In measuring the model's performance, this study uses accuracy metrics, The Receiver operating characteristic (RoC) and Area Under the Curve (AUC). Accuracy is one of the metrics used to evaluate the performance of a classification model. Accuracy [11] measures how precise the model is in making the correct predictions of all the predictions. Accuracy is calculated by comparing the number of accurate predictions with the total number of predictions. The correct prediction is when the model correctly classifies a data sample according to the actual label or class. Accuracy results are expressed in percentage form, where a value of 100% indicates that the model made all predictions correctly. The formula for calculating accuracy [11] is as follows:

$$\text{Accuracy} = (\text{Number of correct predictions} / \text{Total number of predictions}) * 100, \quad (1)$$

Meanwhile, ROC (Receiver Operating Characteristic) [12] is a graph that describes the performance of the classification model at different thresholds. The ROC graph plots the True Positive Rate (TPR) on the Y-axis and the False Positive Rate (FPR) on the X-axis. ROC provides an overview of the model's ability to discriminate between positive and negative classes. The True Positive Rate (TPR), also known as sensitivity or recall, is the percentage of true positives detected from all true positive samples. TPR can be calculated by the formula:

$$TPR = TP / (TP + FN), \quad (2)$$

Where TP (True Positive) is the number of true positive predictions, and FN (False Negative) is the number of false negative predictions. Meanwhile, the False Positive Rate (FPR) is the percentage of false negatives that are falsely detected from all false negative samples. FPR can be calculated by the formula:

$$FPR = FP / (FP + TN) \quad (3)$$

Where FP (False Positive) is the number of false positive predictions, and TN (True Negative) is the number of true negative predictions.

AUC (Area Under the Curve) [12] is the Area under the ROC curve. AUC is used as a performance evaluation metric for the classification model. AUC is in the range of 0 to 1, where a value of 1 indicates a perfect classification, and a value of 0.5 indicates a random classification. The higher the AUC value, the better the model's performance discriminating between positive and negative classes.

c. Results and Discussion

In this study, the Multi-layer Perceptron (MLP) method is used to predict machine failure in the context of predictive maintenance. AI4I 2020 Predictive Maintenance data are processed and prepared for use in model development. The data is divided into training and testing data with appropriate comparisons in the early stages. Next, the data is normalized or standardized to match the different features.

The MLP model is constructed using the appropriate architecture consisting of input, hidden, and output layers. The number of hidden layers and the number of neurons in each hidden layer are determined based on experiments and the specific requirements of the failure prediction problem. After the model is constructed, training is carried out using the processed training data. The training process involves iteratively adjusting the weights and model parameters using the backpropagation algorithm to optimize model performance. After the model is trained, an evaluation is carried out using confusion matrix. Then Accuracy, ROC and AUC are calculated to measure the model's performance in predicting machine failure.

The results of the accuracy of all experiments can be seen in Table 1. It can be seen in Table 1 that the more training data used, the greater the accuracy of the resulting model. The accuracy value of data testing using 90% training data reaches 96%. Meanwhile, the lowest accuracy is obtained when the training data used is only 70%, whereas the accuracy of the data testing results gets 94%.

Furthermore, other metrics, namely RoC and AUC, also show the same thing. The RoC graph of all experiments can be seen in Figure 1. From the ROC graph for all experiments, the AUC value can be derived. The AUC value for all experiments can be seen in Table 2. In line with the high accuracy value, the AUC of data testing from experiments using 90% of the training data is 0.99 or almost perfect, close to 1. These results show that the model built is very precise. Meanwhile, the other AUC results for the proportion of training and testing data 80:20 and 70:30 also offer the same values. The AUC value of data testing for the proportion 80:20 is 0.99, while for the proportion 70:30, the AUC value reaches 0.97.

Compared with the previous research conducted by [idrus], namely on the use of SVM to detect machine failures with data testing accuracy reaching 88%, the MLP here can outperform the research results. It is shown from the three metrics used that the machine failure detection model built using MLP can provide excellent accuracy. This is demonstrated by the accuracy value reaching 96% and the AUC of 0.99. The results of using the MLP method show an accurate and reliable level of prediction in carrying out predictive maintenance. The performance model is evaluated based on the relevant evaluation metrics, and the results show high accuracy and good metric values.

Table 1. Accuracy results of each trial

Experiment	Accuracy of Training	Accuracy of Testing
Train : Test = 90 : 10	91%	96%
Train : Test = 80 : 20	91%	95%

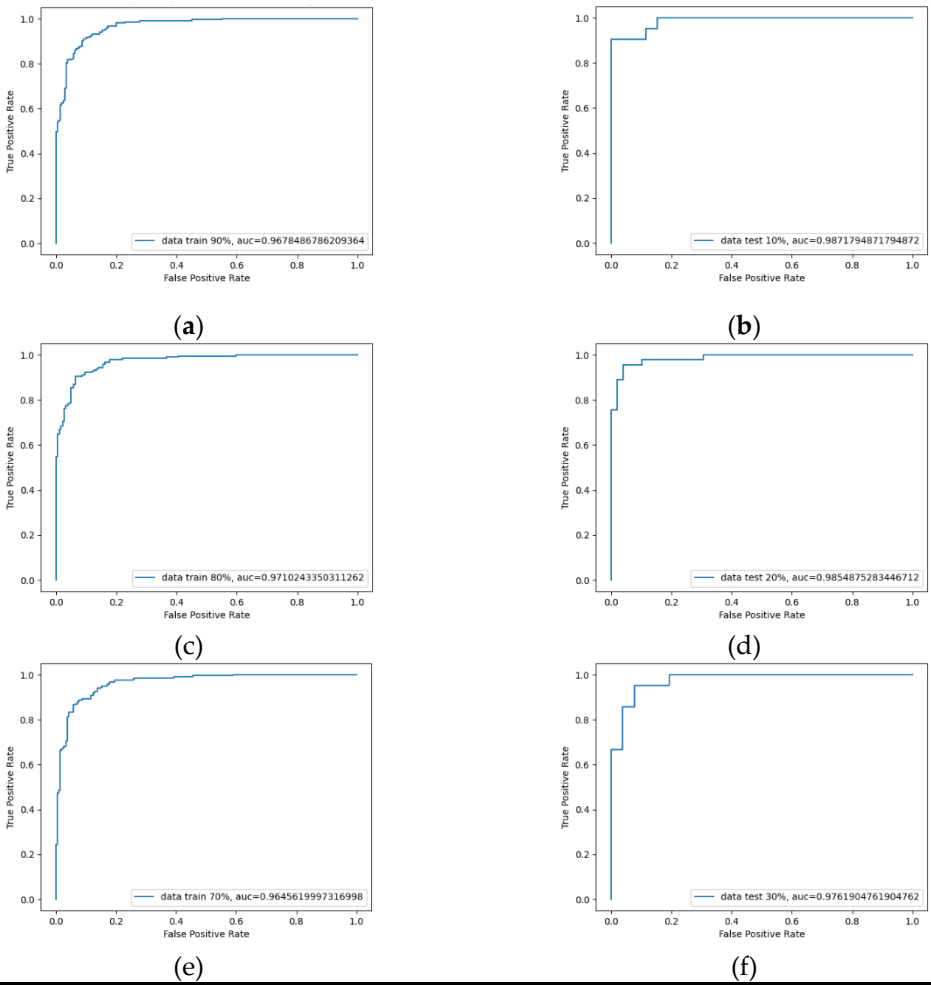

Train : Test = 70 : 30	90%	94%

Figure 1. RoC results from all experiments: (a) RoC Data Training 90%; (b) RoC Data Testing 10%; (c) RoC Data Training 80%; (d) RoC Data Testing 20%; (e) RoC Data Training 70%; (f) RoC Data Testing 30%.

Table 2. AUC results of each trial

Experiment	AUC of Training	AUC of Testing
Train : Test = 90 : 10	0.97	0.99
Train : Test = 80 : 20	0.97	0.99
Train : Test = 70 : 30	0.96	0.97

By using the MLP method, it can be expected that more effective predictive maintenance can be carried out in anticipation of machine failure. This model can extract complex patterns in sensor data and provides reliable predictions about possible failures. However, it should be noted that using an MLP also has some drawbacks. This method requires extensive, high-quality training data and sufficient computational resources to train and implement the model efficiently. In addition, interpreting results from deep learning models can be more complex than straightforward statistical methods.

4. Conclusions

This study uses the deep learning Multi-layer Perceptron (MLP) method to predict machine failure in the context of predictive maintenance. The results of all experiments can be summarized as follows:

1. This method shows a level of prediction that is quite accurate and reliable in identifying machine failures by utilizing operational data and relevant sensors. The accuracy value obtained reaches 96%, and the Area Under Curve value reaches 0.99.
2. Compared with other methods, such as Support Vector Machine (SVM), MLP can extract complex patterns in the data and study non-linear relationships that may exist in the data to provide better performance.

In conclusion, using the MLP method can provide accurate and reliable predictions in carrying out predictive maintenance. However, the drawbacks and complexities of this method must be considered in its application.

Funding: This research was funded by Politeknik Negeri Jakarta.

Conflicts of Interest: The authors declare no conflict of interest.

References

1. Carvalho TP, Soares FA, Vita R, Francisco RD, Basto JP, Alcalá SG. A systematic literature review of machine learning methods applied to predictive maintenance. Computers & Industrial Engineering. 2019 Nov 1;137:106024.
2. Dalzochio J, Kunst R, Pignaton E, Binotto A, Sanyal S, Favilla J, Barbosa J. Machine learning and reasoning for predictive maintenance in Industry 4.0: Current status and challenges. Computers in Industry. 2020 Dec 1;123:103298.
3. Li H, Parikh D, He Q, Qian B, Li Z, Fang D, Hampapur A. Improving rail network velocity: A machine learning approach to predictive maintenance. Transportation Research Part C: Emerging Technologies. 2014 Aug 1;45:17-26.
4. Kanawaday A, Sane A. Machine learning for predictive maintenance of industrial machines using IoT sensor data. In2017 8th IEEE international conference on software engineering and service science (ICSESS) 2017 Nov 24 (pp. 87-90). IEEE.
5. Amruthnath N, Gupta T. A research study on unsupervised machine learning algorithms for early fault detection in predictive maintenance. In2018 5th international conference on industrial engineering and applications (ICIEA) 2018 Apr 26 (pp. 355-361). IEEE.
6. Gohel HA, Upadhyay H, Lagos L, Cooper K, Sanzetenea A. Predictive maintenance architecture development for nuclear infrastructure using machine learning. Nuclear Engineering and Technology. 2020 Jul 1;52(7):1436-42.
7. Sharma N, Sidana T, Singhal S, Jindal S. Predictive maintenance: Comparative study of machine learning algorithms for fault diagnosis. Available at SSRN 4143868. 2022 Jun 22.
8. Assagaf I, Sukandi A, Abdillah AA, Arifin S, Ga JL. Machine Predictive Maintenance by Using Support Vector Machines. Recent in Engineering Science and Technology. 2023 Jan 1;1(01):31-5.
9. Matzka S. AI4I 2020 predictive maintenance dataset. UCI Machine Learning Repository. 2020.
10. Torcianti A, Matzka S. Explainable artificial intelligence for predictive maintenance applications using a local surrogate model. In2021 4th International Conference on Artificial Intelligence for Industries (AI4I) 2021 Sep 20 (pp. 86-88). IEEE.
11. Gorunescu F. Data Mining: Concepts, models and techniques. Springer Science & Business Media; 2011 Mar 10.
12. Lätti S, Niinivehmas S, Pentikäinen OT. Rocker: Open source, easy-to-use tool for AUC and enrichment calculations and ROC visualization. Journal of cheminformatics. 2016 Dec;8(1):1-5.

RiESTech
Recent in Engineering Science and Technology

MBI

Article

Anomaly Response Spectrum of Various Cities in Indonesia Based on SNI 1726:2019

Anis Rosyidah [1,*], Ulil Albab [1], Rinawati [1], I Ketut Sucita [1], Latha M. S [2]

[1] Department of Civil Engineering, Politeknik Negeri Jakarta, Depok 16425, Indonesia
[2] Department of Civil Engineering Sri Venkateshwara College of Engineering, Bangalore, India
* Correspondence: anis.rosyidah@sipil.pnj.ac.id

Abstract: Response spectra that happened anomaly is seen after SNI 1726:2012 and SNI 1726:2019 pub-lished, this condition has happened because the value of response spectrum design is SE < SD < SC, SD < SE < SC, or SD < SC < SE, if this in normal condition, the value of response spectrum is SC < SD < SE. With applied methods and procedures found by Kircher & Associates (2015) they adjust the formula S_{MS} & S_{M1} wished response spectrum becomes normal. In this research, comparing spectrum response, with spectrum response with treatment, and comparing the value SDS dan SD1. From this research, it was found that there was a decrease in seismic loading on hard soil (SC) and an increase in medium soil (SD) and soft soil (SE).

Keywords: Anomaly; Kircher & Associates; Spectrum Response

Citation:. Rosyidah, A., Albab, U., Rinawati, Sucita, I. K., & Latha, M. S., (2023). The Spectra Response Anomaly of Various Cities in Indonesia Based on SNI 1726:2019. Recent in Engineering Science and Technology, 1(03), 32–48. https://doi.org/10.59511/riestech.v1i03.25

Academic Editor: Iwan Susanto

Received: 26 May 2023
Accepted: 12 June 2023
Published: 1 July 2023

Publisher's Note: MBI stays neutral with regard to jurisdictional claims in published maps and institutional affiliations.

1. Introduction

Earthquakes are disasters that cannot be avoided and accurately predicted when and where they will occur. Indonesia is a country with high earthquake intensity due to its location around the convergence of three tectonic plates: the Indo-Cina plate, the Indo-Australian plate, and the Philippine plate [1][2]. The impact of ground acceleration during earthquakes needs to be considered in the design of buildings and infrastructure. During an earthquake, buildings will experience shaking on the ground surface, leading to their destruction. Therefore, structural design regulations that accommodate earthquake loads are essential to reduce the damage caused by earthquakes in Indonesia [3][4].

In Indonesia, there are already earthquake-resistant building regulations that are updated every five years. Indonesia has had earthquake regulations starting from the Indonesian Load Regulation (PPI) in 1970, the Indonesian Earthquake-Resistant Building Planning Regulation (PPTI-UG) in 1983, SNI 1726:2002 - Standard for Earthquake Resistant Building Planning, SNI 1726:2012 - Guidelines for Earthquake Resistance Planning for Building and Non-Building Structures, and SNI 1726:2019 - Guidelines for Earthquake Resistance Planning for Building and Non-Building Structures. These regulations are based on the update of the National Seismic Map, which resulted in the Seismic Source and Hazard Map of Indonesia in 2017. This map is an enhancement of the Seismic Source Map in 2010 [5][6][7]. The increase in seismic sources will affect the magnitude of earthquake forces in earthquake-resistant building design [8]

Since the implementation of SNI 1726:2012 and SNI 1726:2019, many locations have been found to exhibit anomalous response spectra. These anomalies occur in the design for short periods (SDS) and are divided into three types as follows: Type I anomaly is SE < SD < SC, Type II anomaly is SD < SE < SC, and Type III anomaly is SD < SC < SE [4][5]. Here, SE represents earthquake acceleration on soft ground conditions, SD is earthquake acceleration on medium ground conditions, and SC is earthquake acceleration on hard ground conditions [6][9][10].

Response spectra represent a graph showing the relationship between earthquake acceleration Sa (y-axis) and vibration period T in the x-direction. The design response spectra referring to SNI 1726:2019 in various cities in Indonesia have experienced many anomalies [9][11]. Based on this condition, it is essential to determine the percentage of difference in earthquake acceleration on the design response spectra for soft, medium, and hard ground conditions during anomalies and after normalization using the Kircher & Associates method. These results can serve as considerations and references for structural designers to determine planned earthquake loads.

1.1. Respon Spektra

The text discusses the process of creating design response spectra according to SNI 1726:2019 and ASCE 7-16, along with the parameters of earthquake acceleration SS and S1 obtained from MCER (Maximum Considered Earthquake Response) maps.

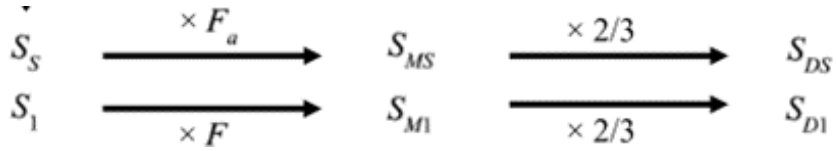

Figure 1. Shows a schematic illustration of the process of creating design response spectra.

The earthquake acceleration parameters, S_s and S_1, are mapped values obtained from the MCER map. To obtain the values of S_s and S_1 at specific latitude and longitude coordinates, interpolation is performed from the four nearest points on the grid. In this study, the website http://rsa.ciptakarya.pu.go.id/2021/ is used to determine the values of SS and S1, following SNI 1726:2019. These values can be obtained from the MCER map for short periods of 0.2 secondsGambar 1 memperlihatkan ilustrasi skematik pembuatan respon spektra desain menurut SNI 1726:2019 dan ASCE 7-16 [11][12].

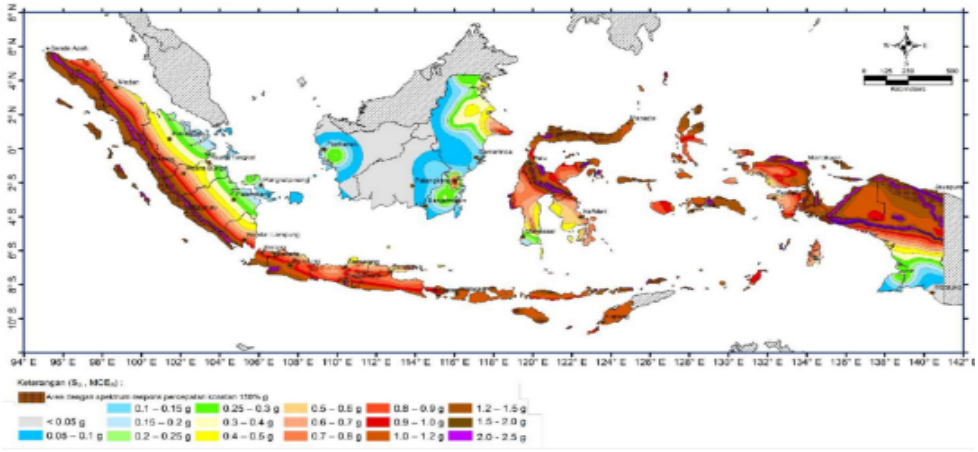

Figure 2. Depicts the Map of Spectrum Acceleration Response for 0.2 seconds 〖MCE〗_R (SNI 1726:2019) [11].

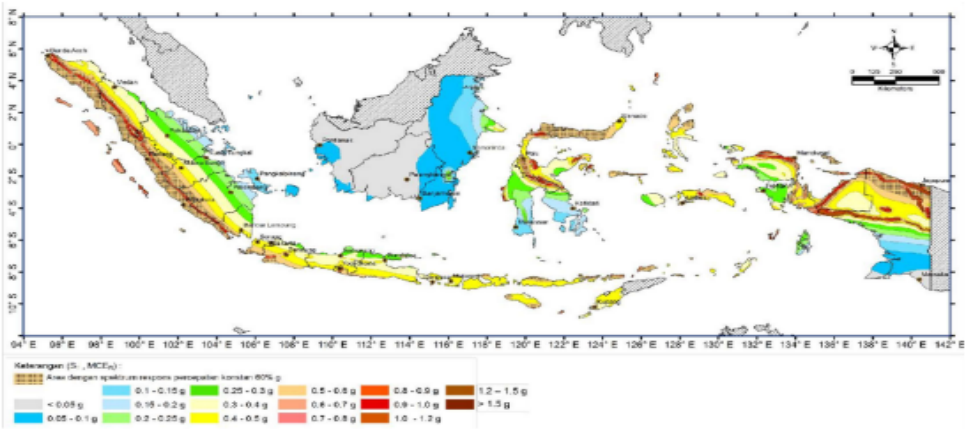

Figure 3. 1-second Response Spectrum Acceleration Map 〖MCE〗_R (SNI 1726:2019) [11]

Based on the provided text, it discusses the coefficients for site amplification Fa and Fv, and the differences between SNI 1726:2019 and ASCE 7-16. SNI 1726:2019 adopted the results of a study from the Pacific Earthquake Engineering Research (PEER), which shows slight differences compared to ASCE 7-16. Research has identified weaknesses in the seismic design procedures ELF (Equivalent Lateral Force) and MSRA (Modal Spectral Response Acceleration) in ASCE 7, particularly regarding the use of two response periods (short period and 1.0-second period) to determine seismic forces in the design [14][15]. Kircher & Associates recommended this research to improve the seismic design requirements of NEHRP 2015 and ASCE 7-16 to avoid anomalies in the response spectra [14]. There are two parameters, Ca and Cv, for adjusting the shape of the response spectra, which are shown in Table 3 to Table 6 [9][11].

Table 1. Fa Site Coefficient [11]

Site Class	parameter of acceleration of MCER spectral response in short period (0.2 second)					
	SNI 1726:2019 Ss ≤ 0,25	SNI 1726:2019 Ss = 0,5	SNI 1726:2019 Ss = 0,75	SNI 1726:2019 Ss = 1,0	SNI 1726:2019 Ss = 1,25	SNI 1726:2019 Ss ≥ 1,5
SA	0,8	0,8	0,8	0,8	0,8	0,8
SB	0,9	0,9	0,9	0,9	0,9	0,9
SC	1,3	1,3	1,2	1,2	1,2	1,2
SD	1,6	1,4	1,2	1,1	1,0	1,0
SE	2,4	1,7	1,3	1,1	0,9	0,8
SF	*Site-Specific* (SSA)					

Table 2. Site Coefficient Fv [11]

Site Class	Parameter of MCER Spectral Response Acceleration in 1-Second Period					
	SNI 1726:2019 $S_1 \leq 0,1$	SNI 1726:2019 $S_1 = 0,2$	SNI 1726:2019 $S_1 = 0,3$	SNI 1726:2019 $S_1 = 0,4$	SNI 1726:2019 $S_1 = 0,5$	SNI 1726:2019 $S_1 \geq 0,6$
SA	0,8	0,8	0,8	0,8	0,8	0,8
SB	0,8	0,8	0,8	0,8	0,8	0,8
SC	1,5	1,5	1,5	1,5	1,5	1,4
SD	2,4	2,2	2,0	1,9	1,8	1,7
SE	4,2	3,3	2,8	2,4	2,2	2,0
SF	*Site-Specific* (SSA)					

Table 3. Short Term Spectrum Shape Adjustment Factor 0.2 , Ca [14]

Site Class	Parameter of MCER Spectral Response Acceleration in Short Period (0.2 second)					
	Ss ≤ 0,25	Ss = 0,5	Ss = 0,75	Ss = 1,0	Ss = 1,25	Ss ≥ 1,5
SA	0,9	0,9	0,9	0,9	0,9	0,9
SB	0,9	0,9	0,9	0,9	0,9	0,9
SC	0,9	0,9	0,9	0,9	0,9	0,9
SD	1,0	1,0	1,0	1,0	1,0	1,0
SE	0,95	1,0	1,1	1,15	1,2	1,25
SF	*Site-Specific* (SSA)					

Table 4. Long Term Spectrum Shape Adjustment Factor, Cv for sites with TL greater than or equal to 12 seconds [14]

Site Class	Parameter of MCER Spectral Response Acceleration in 1-Second Period					
	S_1 ≤ 0,1	S_1 = 0,2	S_1 = 0,3	S_1 = 0,4	S_1 = 0,5	S_1 ≥ 0,6
SA	1,0	1,0	1,0	1,0	1,0	1,0
SB	1,0	1,0	1,0	1,0	1,0	1,0
SC	1,0	1,05	1,05	1,05	1,0	1,1
SD	1,0	1,2	1,3	1,35	1,5	1,5
SE	1,0	1,3	1,5	1,75	1,9	2,0
SF	Site-Specific (SSA)					

Table 5. Long Term Spectrum Shape Adjustment Factor, Cv for sites with TL greater than or equal to 8 seconds [14]

Site Class	Parameter of MCER Spectral Response Acceleration in 1-Second Period					
	S_1 ≤ 0,1	S_1 = 0,2	S_1 = 0,3	S_1 = 0,4	S_1 = 0,5	S_1 ≥ 0,6
SA	1,0	1,0	1,0	1,0	1,0	1,0
SB	1,0	1,0	1,0	1,0	1,0	1,0
SC	1,0	1,0	1,0	1,0	1,0	1,05
SD	1,0	1,1	1,15	1,2	1,3	1,4
SE	1,0	1,15	1,35	1,55	1,65	1,8
SF	Site-Specific (SSA)					

Table 6. Long Term Spectrum Shape Adjustment Factor, Cv for sites with TL greater than or equal to 6 seconds [14]

Site Class	Parameter of MCER Spectral Response Acceleration in 1-Second Period					
	S_1 ≤ 0,1	S_1 = 0,2	S_1 = 0,3	S_1 = 0,4	S_1 = 0,5	S_1 ≥ 0,6
SA	1,0	1,0	1,0	1,0	1,0	1,0
SB	1,0	1,0	1,0	1,0	1,0	1,0
SC	1,0	1,0	1,0	1,0	1,0	1,0
SD	1,0	1,05	1,1	1,15	1,2	1,25
SE	1,0	1,05	1,2	1,4	1,5	1,6
SF	Site-Specific (SSA)					

"The coefficient parameters in Table 3-6 are necessary for adjusting the shape of the spectral response that occurs anomalously. Basically, the method of designing the spectral response that occurs anomalously is the same as designing it normally, but there are adjustments as depicted in the schematic in Figure 4 by multiplying the coefficients Ca and Cv [14].

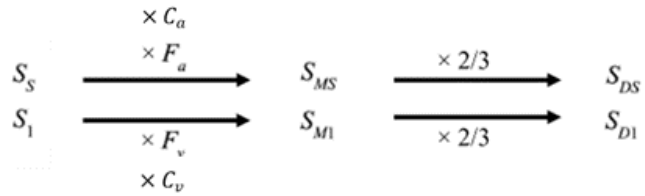

Figure 4. Shows the illustration schematic of the application of the Kircher & Associates design method on the Anomalous Spectral Response [14].

Figure 4: The Process of Applying the Kircher & Associates Design Method on Anomalous Spectral Response Design."Parameter koefisien pada Tabel 3-6 diperlukan untuk penyesuaian bentuk respon spektra yang terjadi anomali. Pada dasarnya cara mendesain respon spektra yang terjadi anomali sama dengan cara mendesain secara normal, tetapi ada penyesuain seperti skematik pada Gambar 4 dengan mengalikan koefisien Ca dan Cv [14].

2. Materials and Experiment Methods

Figure 5 illustrates the process of analyzing the spectral response and the process to make the spectral response normal.

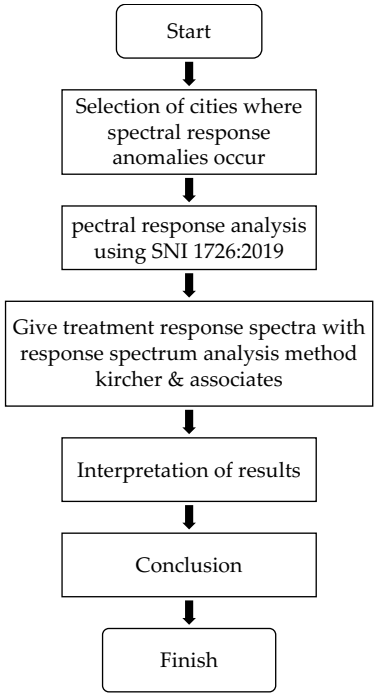

Figure 5. Flowchart of Spectral Response Analysis

The cities selected for this research are earthquake-prone areas, including Sumatra, Java, and Nusa Tenggara islands. The analysis of 15 cities with anomalous spectral responses was conducted using the website http://rsa.ciptakarya.pu.go.id/2021/. These 15

selected cities consist of (1) 5 cities with Type I anomalies, (2) 5 cities with Type II anomalies, and (3) 5 cities with Type III anomalies.

The spectral responses experiencing anomalies are then subjected to specific treatments to normalize them. The spectral response is considered normal if the earthquake acceleration for soft soil is greater than that of medium soil, and medium soil acceleration is greater than that of hard soil (SE > SD > SC). The normalization of the spectral response utilizes the spectral response design method introduced by Kircher & Associates, involving the multiplication of coefficients Ca & Cv (Figure 4) as the adjustment factors for short and long-period spectrum shapes [14].

In seismic-resistant building design, it is essential to accommodate the design earthquake loads. One way is to determine the seismic design loads using spectral response acceleration. The spectral response varies for each region and also depends on the soil site class, resulting in different accelerations. The creation of the design spectral response requires data in the form of acceleration parameters and site coefficients. The acceleration parameters obtained from the spectral acceleration map via the website http://rsa.ciptakarya.pu.go.id/2021/ are presented in Table 7 [16].

Table 1. Coefficient Site 15 cities

No	City	Coefficient S_s	Coefficient S_1
1	Banda Aceh	1.37	0.60
2	Bengkulu	1.12	0.51
3	Mataram	0.96	0.38
4	Padang	1.35	0.60
5	Yogyakarta	1.28	0.47
6	Bogor	0.88	0.36
7	Denpasar Bali	0.98	0.36
8	Jember	0.84	0.40
9	Ngawi	0.90	0.38
10	Salatiga	0.92	0.41
11	Bandar Lampung	0.75	0.32
12	Kebumen	0.85	0.42
13	Kediri	0.84	0.34
14	Malang	0.78	0.33
15	Purwokerto	0.84	0.34

In Table 7, cities numbered 1-5 belong to Type 1 anomalies, numbers 6-10 belong to Type 2 anomalies, and numbers 11-15 belong to Type 3 anomalies.

3. Results and Discussion

This section presents the seismic amplification factor values (Fa and Fv) from various regions experiencing anomalies (Table 8). The spectral responses experiencing anomalies are then normalized using the Kircher & Associates design method presented in Table 9.

Table 8. Coefficient Values F_a and F_v Based on SNI 1726:2019.

No	City	SC		SD		SE	
		F_a	F_v	F_a	F_v	F_a	F_v
1	Banda Aceh	1.2	1.4	1.0	1.7	0.9	2.0
2	Bengkulu	1.2	1.5	1.1	1.8	1.0	2.2
3	Mataram	1.2	1.5	1.1	1.9	1.1	2.5
4	Padang	1.2	1.4	1.0	1.7	0.9	2.0
5	Yogyakarta	1.2	1.5	1.0	1.8	0.9	2.3
6	Bogor	1.2	1.5	1.1	1.9	1.2	2.6
7	Denpasar Bali	1.2	1.5	1.1	1.9	1.1	2.6
8	Jember	1.2	1.5	1.1	1.9	1.2	2.6
9	Ngawi	1.2	1.5	1.1	1.9	1.2	2.5
10	Salatiga	1.2	1.5	1.1	1.9	1.2	2.4
11	Bandar Lampung	1.2	1.5	1.2	2.0	1.3	2.7
12	Kebumen	1.2	1.5	1.2	1.8	1.2	2.2
13	Kediri	1.2	1.5	1.2	2.0	1.3	2.6
14	Malang	1.2	1.5	1.2	2.0	1.3	2.7
15	Purwokerto	1.2	1.5	1.2	2.0	1.2	2.6

Table 9. Coefficient Values Fa and Fv After Normalization

No	City	SC		SD		SE	
		F_a	F_v	F_a	F_v	F_a	F_v
1	Banda Aceh	1.2	1.402	1.2	1.702	1.2	2.004
2	Bengkulu	1.2	1.5	1.2	1.8	1.2	2.2
3	Mataram	1.2	1.5	1.2	1.916	1.2	2.464
4	Padang	1.2	1.4	1.2	1.7	1.2	2
5	Yogyakarta	1.2	1.5	1.2	1.835	1.2	2.27
6	Bogor	1.2	1.5	1.2	1.944	1.2	2.576
7	Denpasar Bali	1.2	1.5	1.2	1.94	1.2	2.56
8	Jember	1.2	1.5	1.142	1.943	1.184	2.572
9	Ngawi	1.2	1.5	1.2	1.918	1.2	2.47
10	Salatiga	1.2	1.5	1.2	1.886	1.2	2.372
11	Bandar Lampung	1.2	1.5	1.2	1.98	1.2	2.72
12	Kebumen	1.2	1.5	1.2	1.964	1.2	2.656
13	Kediri	1.2	1.5	1.2	1.961	1.2	2.644
14	Malang	1.2	1.5	1.2	1.969	1.2	2.676
15	Purwokerto	1.2	1.5	1.166	1.961	1.232	2.644

The parameters of acceleration response spectra at short period (S_MS) and 1.0-second period (S_M1) are adjusted according to the site classification and seismic amplification factor. To determine the anomalies that occur, three site class conditions are needed: hard soil (SC), medium soil (SD), and soft soil (SE) [17].

Table 10 presents the values of acceleration response spectra parameters that experience anomalies at short period (S_MS) and 1.0-second period (S_M1). These values are the result of multiplying the site classification with the seismic amplification factor based on SNI 1726:2019. Table 11 shows the values of acceleration response spectra parameters at

short period (S_MS) and 1.0-second period (S_M1). These results are a step towards normalization using the Kircher & Associates method.

Table 10. Values of S_MS and S_M1 Based on SNI 1726:2019.

No	City	SC		SD		SE	
		S_{MS}	S_{M1}	S_{MS}	S_{M1}	S_{MS}	S_{M1}
1	Banda Aceh	1.645	0.838	1.371	1.018	1.168	1.198
2	Bengkulu	1.348	0.761	1.180	0.913	1.125	1.115
3	Mataram	1.151	0.576	1.071	0.736	1.086	0.946
4	Padang	1.625	0.839	1.354	1.018	1.162	1.198
5	Yogyakarta	1.540	0.698	1.283	0.853	1.138	1.056
6	Bogor	1.058	0.534	1.012	0.692	1.053	0.917
7	Denpasar Bali	1.172	0.540	1.084	0.698	1.093	0.922
8	Jember	1.004	0.593	0.956	0.767	0.991	1.016
9	Ngawi	1.076	0.574	1.023	0.733	1.060	0.945
10	Salatiga	1.107	0.621	1.043	0.781	1.072	0.982
11	Bandar Lampung	0.900	0.480	0.900	0.634	0.975	0.870
12	Kebumen	1.022	0.635	0.987	0.759	1.038	0.925
13	Kediri	0.956	0.509	0.941	0.665	1.006	0.896
14	Malang	0.940	0.497	0.929	0.652	0.997	0.886
15	Purwokerto	1.002	0.509	0.974	0.665	1.029	0.896

Table 11. Normalized Values of S_MS and S_M1

No	City	SC		SD		SE	
		S_{MS}	S_{M1}	S_{MS}	S_{M1}	S_{MS}	S_{M1}
1	Banda Aceh	1.481	0.921	1.645	1.526	2.014	2.394
2	Bengkulu	1.213	0.766	1.348	1.326	1.583	2.127
3	Mataram	1.036	0.605	1.151	0.987	1.314	1.618
4	Padang	1.462	0.922	1.625	1.527	1.984	2.395
5	Yogyakarta	1.386	0.71	1.54	1.207	1.858	1.95
6	Bogor	0.953	0.561	1.058	0.919	1.192	1.504
7	Denpasar Bali	1.055	0.567	1.172	0.929	1.343	1.521
8	Jember	0.904	0.622	0.956	1.02	1.119	1.669
9	Ngawi	0.968	0.602	1.076	0.974	1.215	1.612
10	Salatiga	0.996	0.652	1.107	1.02	1.255	1.506
11	Bandar Lampung	0.81	0.504	0.9	0.83	0.99	1.349
12	Kebumen	0.875	0.529	0.972	0.871	1.081	1.426
13	Kediri	0.861	0.534	0.956	0.877	1.061	1.432
14	Malang	0.846	0.521	0.94	0.857	1.04	1.397
15	Purwokerto	0.902	0.534	0.974	0.877	1.149	1.432

Tables 10 and 11 represent the acceleration spectrum design parameters used to create the design spectrum response graph. This graph is utilized to determine the planned earth-

quake loads in the form of base shear forces caused by the earthquake. The design spectrum response is obtained by dividing the surface acceleration response parameters (SMS and SM1) by a 1.5 margin against collapse [8][18].

Table 12 shows the values of the spectral acceleration parameters at short period (SDS) and 1.0-second period (SD1) that experience anomalies. Table 13 contains the values of the spectral acceleration parameters at short period (SDS) and 1.0-second period (SD1) that have been normalized using the Kircher & Associates method.

Table 12. Values of SDS and SD1 Based on SNI 1726:2019.

No	City	SC		SD		SE	
		S_{DS}	S_{D1}	S_{DS}	S_{D1}	S_{DS}	S_{D1}
1	Banda Aceh	1.097	0.559	0.914	0.679	0.778	0.799
2	Bengkulu	0.898	0.507	0.787	0.608	0.750	0.744
3	Mataram	0.767	0.384	0.714	0.490	0.724	0.631
4	Padang	1.083	0.559	0.903	0.679	0.775	0.799
5	Yogyakarta	1.026	0.465	0.855	0.569	0.759	0.704
6	Bogor	0.706	0.356	0.675	0.461	0.702	0.611
7	Denpasar Bali	0.782	0.360	0.722	0.466	0.728	0.614
8	Jember	0.670	0.395	0.637	0.512	0.661	0.677
9	Ngawi	0.717	0.383	0.682	0.489	0.707	0.630
10	Salatiga	0.738	0.414	0.695	0.520	0.715	0.654
11	Bandar Lampung	0.600	0.320	0.600	0.422	0.650	0.580
12	Kebumen	0.681	0.424	0.658	0.759	0.692	0.616
13	Kediri	0.638	0.339	0.628	0.443	0.671	0.598
14	Malang	0.626	0.331	0.620	0.434	0.665	0.591
15	Purwokerto	0.668	0.339	0.649	0.443	0.686	0.598

Table 13. Normalized Values of SDS and SD1

No	City	SC		SD		SE	
		S_{DS}	S_{D1}	S_{DS}	S_{D1}	S_{DS}	S_{D1}
1	Banda Aceh	0.987	0.614	1.097	1.017	1.343	1.596
2	Bengkulu	0.809	0.511	0.898	0.884	1.055	1.418
3	Mataram	0.690	0.403	0.767	0.658	0.876	1.079
4	Padang	0.975	0.614	1.083	1.018	1.322	1.597
5	Yogyakarta	0.924	0.473	1.026	0.805	1.238	1.300
6	Bogor	0.635	0.374	0.706	0.613	0.795	1.003
7	Denpasar Bali	0.703	0.378	0.782	0.619	0.895	1.014
8	Jember	0.603	0.415	0.637	0.680	0.746	1.112
9	Ngawi	0.645	0.402	0.717	0.649	0.810	1.075
10	Salatiga	0.664	0.434	0.738	0.680	0.837	1.004
11	Bandar Lampung	0.540	0.336	0.600	0.553	0.660	0.899
12	Kebumen	0.583	0.353	0.648	0.871	0.721	0.950
13	Kediri	0.574	0.356	0.638	0.585	0.707	0.955

14	Malang	0.564	0.348	0.626	0.572	0.693	0.932
15	Purwokerto	0.601	0.356	0.649	0.585	0.766	0.955

The normalization of the site class spectral response graph for Hard Soil (SC) shows a decrease in SDS values by an average of 10%, and an increase in SD1 values by an average of 5%. For Medium Soil (SD), the S_DS values increase by an average of 7.74%, and the SD1 values increase by an average of 34.95%. For Soft Soil (SE), the S_DS values increase by an average of 25.06%, and the SD1 values increase by an average of 69.99%.

The results of the plot of the spectral response anomalies and the normalized spectral responses from 15 cities are presented together in Figures 6 - 20. The spectral response anomalies are depicted with solid lines, while the treated design spectral responses are presented with dashed lines. The curves in blue, yellow, and red respectively represent Soft Soil (SE), Medium Soil (SD), and Hard Soil (SC) site classes.

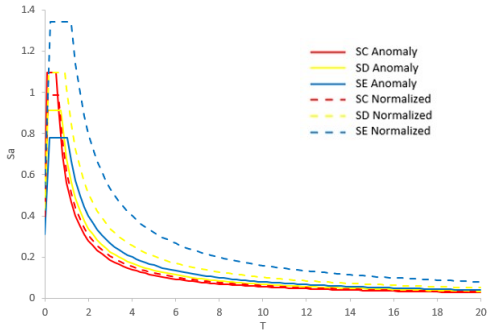

Figure 6. Design Spectral Response of Banda Aceh City

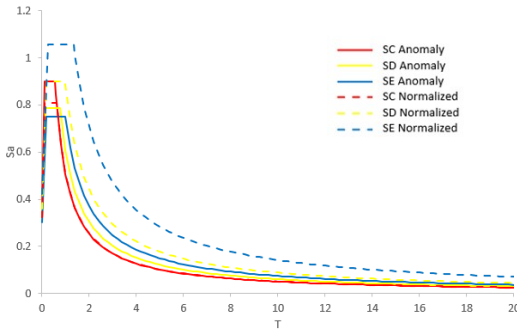

Figure 7. Design Spectral Response of Bengkulu City

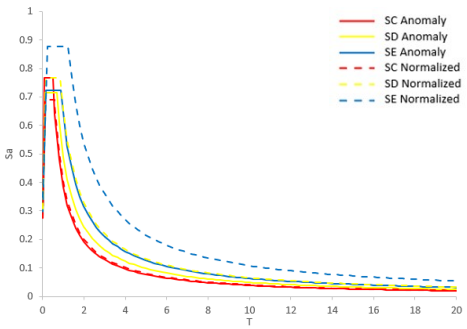

Figure 8. Design Spectral Response of Mataram City

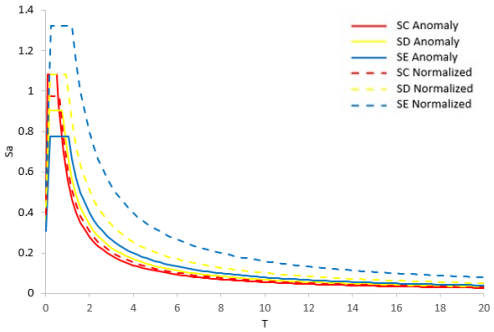

Figure 9. Design Spectral Response of Padang City

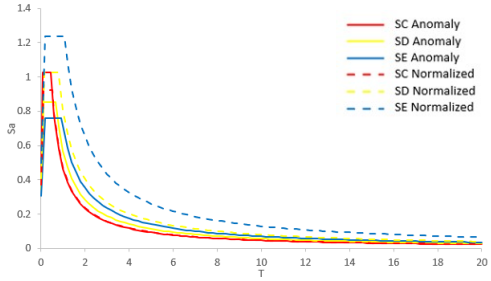

Figure 10. Design Spectral Response of Yogyakarta City

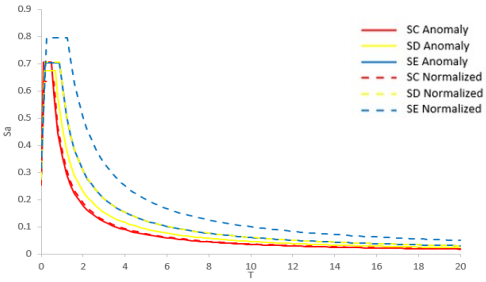

Figure 11. Design Spectral Response of Bogor City

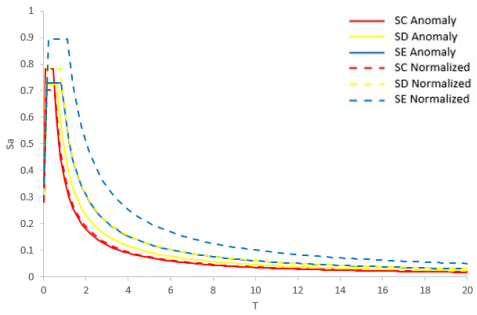

Figure 12. Design Spectral Response of Bali City

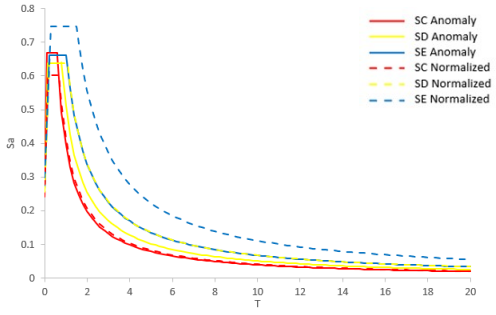

Figure 13. Design Spectral Response of Jember City

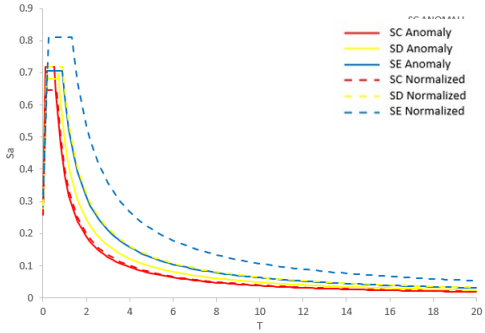

Figure 14. Design Spectral Response of Ngawi City

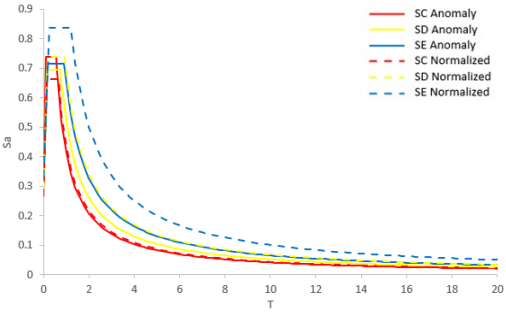

Figure 15. Design Spectral Response of Salatiga City

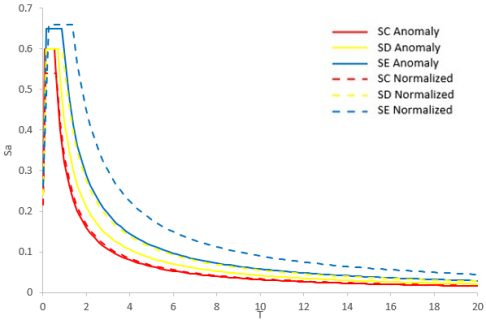

Figure 16. Design Spectral Response of Bandar Lampung City

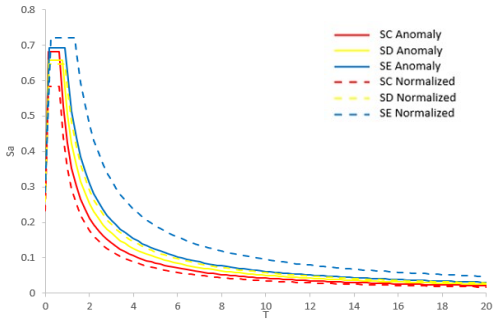

Figure 17. Design Spectral Response of Kebumen City

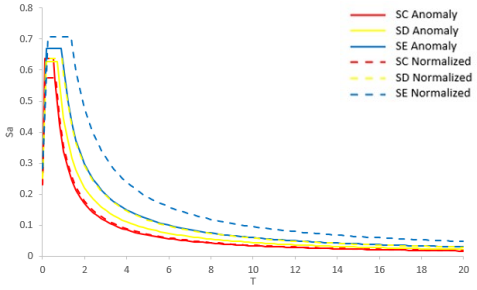

Figure 18. Design Spectral Response of Kediri City

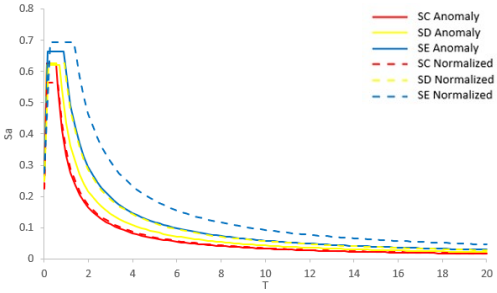

Figure 19. Design Spectral Response of Malang City

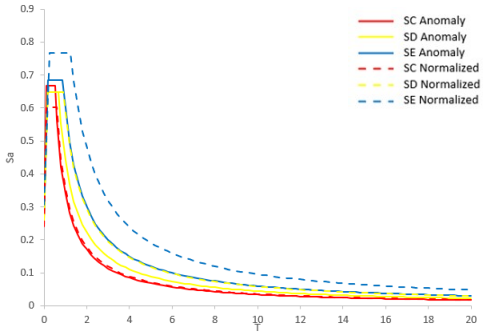

Figure 20. Design Spectral Response of Purwokerto City

The text describes the spectral response graphs from Figure 6 to Figure 20, indicating anomalies in earthquake-prone cities where the Ss value is above 0.75 g [9][19]. After normalization, the spectral response graphs appear normal, with earthquake accelerations in the Hard Soil (SC) site class being lower than those in the Medium Soil (SD) site class, which in turn are lower than those in the Soft Soil (SE) site class.

The results of normalizing the spectral response for Medium Soil (SD) and Soft Soil (SE) using the Kircher & Associates design method show a significant increase in earthquake acceleration compared to when anomalies were present. On the other hand, the normalization of the spectral response for Hard Soil (SC) results in a decrease in earthquake acceleration compared to when anomalies were present. Based on the spectral response graphs in Figures 6 to 10, it is observed that anomalies of Type 1 experience the most significant changes after normalization, followed by Type II anomalies (Figures 11-15), and finally Type III anomalies (Figures 16-20) [9][19].

4. Conclusions

The text discusses the anomalies observed in the design spectral response graphs for 15 earthquake-prone cities, categorized into three types: (1) Type I anomaly where SE < SD < SC, (2) Type II anomaly: SD < SE < SC, and (3) Type III anomaly: SD < SC < SE. The spectral responses experiencing anomalies were normalized using the Kircher & Associates method. The normalization process resulted in a decrease in earthquake acceleration for Hard Soil (SC) and an increase in earthquake acceleration for Medium Soil (SD) and Soft Soil (SE).

In earthquake-prone areas in Indonesia, it is common to experience anomalies in the spectral response graphs. These graphs are used to determine the planned earthquake loads for structural design. To ensure that a location experiences anomalies or not, it is essential to display the design spectral responses for all soil conditions. Anomalous spectral responses can be identified by plotting all soil types in one graph.

The consequences of errors arising from anomalous design spectral responses without normalization can be catastrophic. For Medium and Soft Soil site classes, the earthquake acceleration values for the spectral responses experiencing anomalies are lower than those that have been normalized. As a result, the design earthquake loads become smaller. If a major earthquake occurs that exceeds the design earthquake loads, the building may collapse. It is crucial to properly account for anomalies and perform normalization to ensure the safety and stability of structures in earthquake-prone areas.

References

1. BMKG, "Kejadian Gempa Bumi Merusak Di Indonesia Tahun 2022," *Kementerian Energi dan Sumber Daya Mineral Badan Geologi*, 2023. [Online]. Available: https://vsi.esdm.go.id/index.php/kegiatan-pvmbg/kegiatan-diseminasi-informasi/4041-kejadian-gempa-bumi-merusak-di-indonesia-tahun-2022.
2. J. Supriyanto *et al.*, "'Sistem Informasi Gempa Bumi Menggunakan data XML Berbasis pengolahan Teks Parsing dan Concatenation,'" *Telematika*, vol. 16, no. 1, pp. 35–42, 2019.
3. A. Wicaksana and A. Rosyidah, "PEMBANDINGAN DESAIN BANGUNAN TAHAN GEMPA MENGGUNAKAN SNI 1726 : 2012 DAN SNI 1726:2019," no. 11, 2020.
4. J. P. Stewart and E. Seyhan, "Semi-empirical nonlinear site amplification and its application in NEHRP site factors," *Berkeley, United States Am. Pacific Earthq. Eng. Res. Cent.*, no. November, 2013.
5. P. S. G. Nasional, *Peta Sumber Dan Bahaya Gempa Indonesia Tahun 2017*. 2017.
6. S. Sutjipto and I. Sumeru, "Comparison of the RSNI 1726:2018 and the SNI 1726:2012 design response spectra of 17 major cities in Indonesia," *IOP Conf. Ser. Mater. Sci. Eng.*, vol. 650, no. 1, pp. 0–10, 2019.
7. C. B. Surya Permana, "Design Response Spectra Based on Earthquake Hazard Maps and Specific Soil Properties at Indonesian Ports According to SNI 1726 2019," *J. Tek. Sipil*, vol. 17, no. 1, pp. 41–54, 2021.
8. M. Sitompul, H. M. Pasaribu, and T. Oktaviani, "Studi Perbandingan Spektrum Respons Desain SNI 1726:2019 terhadap SNI 1726:2012 di Provinsi Sumatera Utara," *J. Tek. Sipil*, vol. 11, no. 1, pp. 30–39, 2022.
9. S. Sutjipto and I. Sumeru, "Anomaly Phenomena on the New Indonesian Seismic Code SNI 1726:2019 Design Response Spectra," in *6th International Conference on Civil, Offshore and Environmental Engineering, ICCOEE 2020*, 2021, vol. 132, pp. 375–384.
10. S. Sutjipto, "Anomali Spektrum Respons Desain SNI 1726 : 2012," in *Prosiding Seminar dan Pameran Himpunan Ahli Konstruksi Indonesia (HAKI) 2015*, 2015, pp. 1–14.
11. SNI 1726, *Tata Cara Perencanaan Ketahanan Gempa untuk Struktur Bangunan Gedung dan Nongedung*. Bandung: Badan Standardisasi Indonesia, 2019, p. 254.
12. ASCE 7-16, *Minimum Design Loads for Buildings and Other Structures (ASCE/SEI 7-16)*. 2016.
13. M. Irsyam, B. M. Hutapea, and I. Imran, "Zonasi Hazard Gempa Bumi untuk Wilayah Jakarta," *J. Tek. Sipil*, vol. 24, no. 2, pp. 159–166, 2017.
14. Kircher & Associates, "Investigation of an identified short-coming in the seismic design procedures of ASCE 7-10 and development of recommended improvements for ASCE 7-16," *Seism. Des. Proced. Study*, 2015.
15. I. W. Sengara *et al.*, "New 2019 Risk-Targeted Ground Motions for Spectral Design Criteria in Indonesian Seismic Building Code," *E3S Web Conf.*, vol. 156, p. 03010, 2020.
16. 1726-2019 SNI, *Tata Cara Perencanaan Ketahanan Gempa untuk Struktur Bangunan Gedung dan Non Gedung*. Badan Standarisasi Nasional, Jakarta, 2019.
17. J. X. Zhao *et al.*, "Attenuation relations of strong ground motion in Japan using site classification based on predominant period," *Bull. Seismol. Soc. Am.*, vol. 96, no. 3, pp. 898–913, 2006.
18. A. Cipta, P. Cummins, M. Irsyam, and S. Hidayati, "Basin resonance and seismic hazard in jakarta, Indonesia," *Geosci.*, vol. 8, no. 4, Apr. 2018.
19. S. Sutjipto, "Perbandingan Spektrum Respons Desain RSNI 1726 : 2018 dan SNI 1726-2012 Pada 17 Kota Besar Di Indonesia," in *Konferensi Nasional Teknik Sipil ke-12 2018*, 2018, pp. 1–7.

RiESTech
Recent in Engineering Science and Technology

MBI

Article

The Effect of 5wt.% and 10wt.% Salacca Frond Fiber Addition on Kevlar and Carbon Fiber Reinforced Epoxy using Vacuum Assisted Resin Transfer Molding (VARTM) Method for Bulletproof Vest Application

Vina Nanda Garjati [1,*], Vika Rizkia [1], Nur Agnes Aggraeni [1], Muslimin [1]

[1] Department of Mechanical Engineering, Politeknik Negeri Jakarta, Depok 16425, Indonesia
* Correspondence: vina.nanda@mesin.pnj.ac.id

Abstract: Bulletproof vests as self-protection for military personnel are generally made from synthetic fiber-reinforced composites. Kevlar and carbon fiber reinforced composites have been able to withstand bullet penetration rates and have lightweight characteristics, but production costs with synthetic fibers are relatively expensive. The use of substitute materials from natural fiber is very potential, due to the abundance of natural fiber, lightweight, and relatively cheap price. One of the potential natural fibers is fiber from the salacca midrib. This study focused on the effect of adding salacca frond fiber on the composite characteristics of Kevlar fiber and carbon fiber, with SiC and Al2O3 fillers. The manufacture of this composite is carried out by the Vacuum Assisted Resin Transfer Molding (VARTM) method. There are 4 variations of fiber volume fractions and fillers as reinforcement added to this composite. From the results of observations with SEM, the results of the matrix and reinforcement are well bound. The ballistic test results show that all variations of test samples can withstand the bullet rate so that it does not penetrate. The results of mechanical tests show that currently the addition of salacca frond fiber has not significantly improved the mechanical properties of the composite

Keywords: Composite; Natural Fiber; Sallaca Frond Fiber; VARTM; Bulletproof Vests

Citation:. Garjati, V. N., Vika Rizkia, Aggraeni , N. A., & Muslimin. (2023). The Effect of 5wt.% and 10wt.% Salacca Frond Fiber Addition on Kevlar and Carbon Fiber Reinforced Epoxy using Vacuum Assisted Resin Transfer Molding (VARTM) Method for Bulletproof Vest Application. Recent in Engineering Science and Technology, 1(03), 45–55. https://doi.org/10.59511/riestech.v1i03.27

Academic Editor: Iwan Susanto

Received: 9 June 2023
Accepted: 26 June 2023
Published: 1 July 2023

Publisher's Note: MBI stays neutral with regard to jurisdictional claims in published maps and institutional affiliations.

1. Introduction

A bulletproof vest is the most common ballistic protection instrument used by military personnel. The ability to have high mobility and effective protection are the main characteristics required for the use of a bulletproof vest[1]. In order to fulfill the function of withstanding penetration and minimizing the impact energy from projectiles, selecting appropriate materials is crucial. Initially, bulletproof vests used in World War I & II were made of metal. However, these vests had the disadvantage of being heavy, which could hinder the mobility of military personnel[2]. This issue has encouraged innovation and curiosity in synthetic composite materials research, which are Kevlar and carbon.

The use of Kevlar fibers in composites has a significant impact on the tensile strength properties. Being incredibly strong and durable, Kevlar fibers have been widely used in various composite applications such as boats, airplanes, racing cars, and even protective clothing. Kevlar fibers are renowned for their high strength, stiffness, and resistance to wear. In composites, Kevlar fibers are typically used as reinforcement to enhance their tensile strength. This is possible because Kevlar fibers can withstand high tensile forces, reducing the risk of material failure and improving the durability and safety of the composite[2]. During the composite production process, Kevlar fibers can be combined with

other materials such as carbon fibers or glass fibers to reinforce the composite. However, the use of Kevlar fibers also has its drawbacks. Kevlar fibers are more expensive than other fibers, leading to higher composite production costs. Additionally, Kevlar fibers exhibit different thermal properties compared to other base materials in the composite, requiring careful consideration during the design and production process[2].

Kevlar and carbon fibers reinforced composites have adequately met the primary criteria for bulletproof vests, which require lightweight and strong materials[3][4]. The utilization of Kevlar fibers in composites can enhance their tensile strength, yet cost and thermal properties must also be taken into account. Therefore, careful calculations and adjustments are necessary to ensure that Kevlar fibers can provide optimal benefits for the composite products.

Due to the abundance and relatively low cost of natural fibers, various research have been developed to study the replacement of synthetic fibers with natural fibers in composite fabrication[5][6][7]. Moreover, these fibers possess low density and reasonably good mechanical properties for application in bulletproof vests[8].

Ning, H. reported that embedding kenaf fibers in polyethylene composites demonstrated a significant increase in tensile strength[9]. A.M.R Azmi performed ballistic tests on the same material, but the results indicated the need for further improvement in material quality to fully withstand bullet penetration[10].

The potential natural fiber for substituting synthetic fibers is Salacca frond fibers, which are extracted from salacca tree. The salak fruit tree is a tropical plant abundant in Indonesia, particularly in the Special Region of Yogyakarta. Various studies have been conducted regarding salacca frond fibers in Indonesia. Yudha, et al., have successfully isolated cellulose from the rachis of the salak fruit tree to produce salacca frond fibers[11][12]. However, further research on the effects of salacca frond fibers as reinforcement in composites for bulletproof vest applications is highly needed. Thus, this study focuses on the manufacturing and analysis of epoxy resin composites reinforced with salacca frond fibers, carbon fibers, and Kevlar fibers, using SiC and Al2O3 fillers through the Vacuum Assisted Resin Transfer Molding (VARTM) method.

2. Materials and Experiment Methods

The composite plates in this research were produced through the Vacuum Assisted Resin Transfer Molding (VARTM) method with symmetrical fiber orientation[13][14]. Several modifications were made to the VARTM method by adding a rigid mold at the top to achieve a smooth surface finish on the upper part and to obtain the desired thickness while ensuring a smooth distribution of resin into the mold. The dimensions of the composite molds used were 25 x 25 x 2 cm, 25 x 25 x 0.25 cm, and 20 x 15 x 1.27 cm. The sequence of fiber arrangement, in consecutive order, was Kevlar fibers with Al_2O_3 filler, salacca frond fibers, carbon fibers, salacca frond fibers, and Kevlar fibers with SiC filler. The four variations of fiber additions in this study are presented in Table 1.

Subsequently, adhesive was sprayed, and all laminate surfaces were covered to ensure airtightness. Then, the resin was injected into the mold, and the samples were left to cure. Characterization performed on the composite samples in this study included impact testing (ASTM D6110-10), tensile testing (ASTM D3039), hardness testing, Scanning Electron Microscope (SEM) analysis, and ballistic testing following the NIJ 0101.06 Level II standard. Ballistic testing was conducted using 9 mm caliber ammunition (MU-1TJ) with a mass of 8 grams and an average velocity of 380 m/s. Additionally, ballistic tests were conducted using 5.56 mm caliber ammunition (MU5-TJ) with a mass of 4 grams and an average velocity of 915 m/s.

Table 1. Variation of fiber in the composite

No.	Salacca Frond Fiber (%)	SiC Filler (%)	Al_2O_3 Filler (%)	Carbon Fiber (%)	Kevlar Fiber (%)
1	10	5	5	10	10
2	5	5	5	10	15
3	2.5	7.5	7.5	2.5	20
4	2.5	5	5	2.5	25

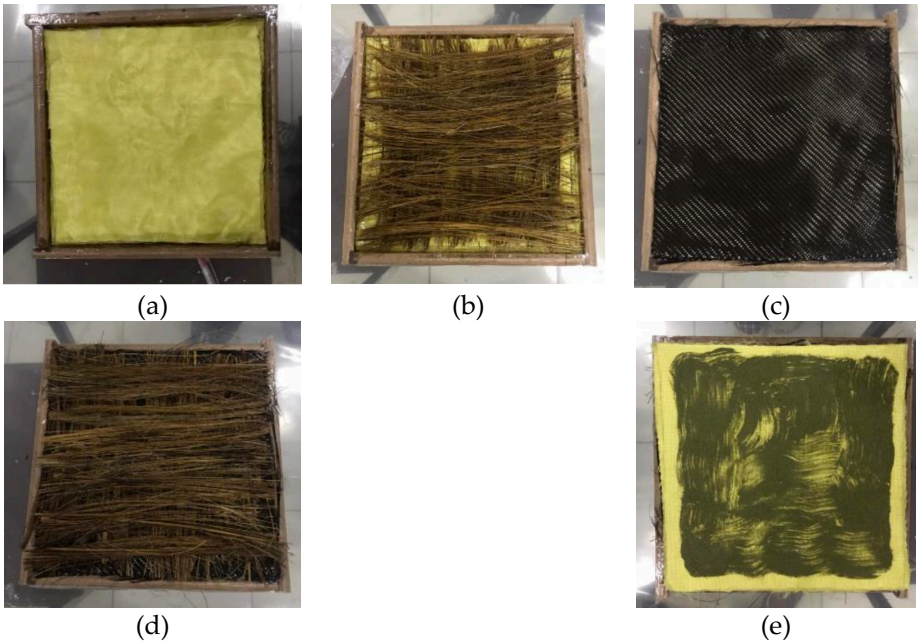

Figure 1. composite fiber arrangement in the mold: (a) Kevlar fibers, (b) salacca palm fibers, (c) carbon fibers, (d) second layer of salacca frond fibers, and (e) Kevlar fibers with Al_2O_3 filler as the top layer

3. Results and Discussion

3.1 Tensile Test Analysis

Tensile testing was performed on 5 specimens for each sample variation. The average tensile strength values of all specimens for each fiber addition variation are depicted in Figure 2. As can be seen, the 1st variation showed the lower tensile test value of 148.59 N/mm^2. Meanwhile, the 4th variation reached the highest tensile test value of 177.91 N/mm2.

Based on the test results, 1st variation with the highest addition of salacca frond fiber of 10wt.%, and the lowest addition of Kevlar fibers of 10wt.%, exhibited the lowest tensile strength compared to the other four variations. On the other hand, 4th variation with the lowest addition of salacca frond fibers of 2.5wt.%, and the highest addition of Kevlar fibers of 25wt.%, showed the highest tensile strength among the four variations.

Tensile strength is greatly influenced by the constituent materials, in this research, the composition of the fiber reinforcements. The significant improvement in tensile strength is attributed to the addition of Kevlar fibers, while the effect of salacca frond fibers addition on enhancing the tensile strength of the material is not yet apparent.

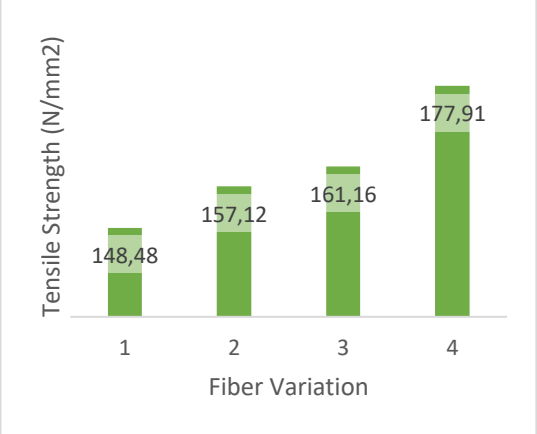

Figure 2. Comparison of Tensile Strength value for all variations

3.2 Hardness Test Analysis

Hardness testing was conducted using the Rockwell method on the F scale with a 1/16-inch indenter size and a force of 60 kgf. The testing involved indenting 5 points on each sample. The average hardness values for all indentations in this research are shown in Figure 3. Figure 3 depicts that the 1st variation showed the lowest hardness test value of 23 HRF. Meanwhile, the 4th variation yielded the highest hardness test value of 49.8 HRF.

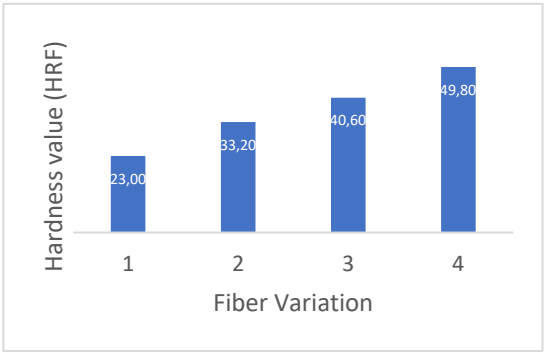

Figure 3. Comparison of hardness value for all variations.

The variation with the highest addition of salacca frond fiber (10wt.%) and the lowest addition of Kevlar fibers (10wt.%) had the lowest hardness value compared to the other four variations. In contrast, the fourth variation with the lowest addition of salacca frond fibers (2.5wt.%) and the highest addition of Kevlar fibers (25wt.%) exhibited the greatest hardness value among the four variations. This phenomenon is due to during the hardness

testing, the tested part is the upper portion composed of SiC and Kevlar fibers. The significant increase in hardness value is predominantly due to the effect of adding Kevlar fibers into the composites.

3.3 Impact Test Analysis

All of the impact test specimens in this research followed the ASTM D 6110-10 standard. The average Impact Strength (IS) values of all fiber variations are presented in Figure 4. Each sample variation consists of 5 (five) impact specimens. Based on Figure 4, it is clearly seen that the average impact strength for the first variation is 0.19 J/mm^2, while the impact strength for the second variation is 0.18 J/mm^2.

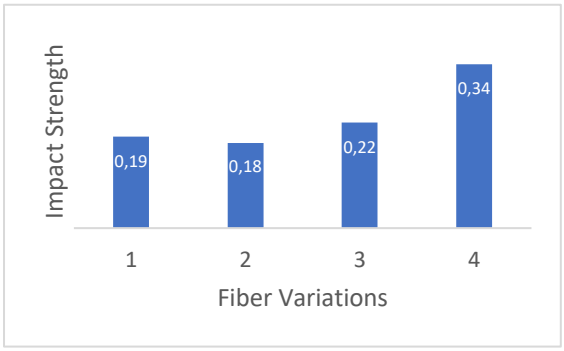

Figure 4. Comparison of impact strength value for all variations.

A higher content of salacca frond fibers will increase the impact resistance of the composite material. This phenomenon is related to the presence of a strong bond between the salacca frond fibers and the matrix, allowing for even energy transfer throughout the fibers. Therefore, an increased amount of salacca frond fibers will result in higher resistance to impact loading. The average impact strength for the third variation is 0.22 J/mm^2, while the impact strength for the fourth variation is 0.34 J/mm^2. The increase in Impact Strength (IS) with the increasing amount of Kevlar fibers in this composite indicates that the Kevlar fiber composition affects the impact strength of materials, whereas a higher Kevlar fiber content enhances the composite material's resistance to impact loading.[15]

3.4 Morphological Analysis

Microstructure observations were conducted using a Scanning Electron Microscope to examine the bond between the matrix and the reinforcement. Based on Figure 5, for the 1st and 2nd variations, debonding (bond detachment failure) is observed. However, the matrix (resin) and reinforcement (fibers) of both specimens are well-bonded as can be seen in Figure 5(a) and (b). In the 3rd variation, fiber pull-out (failure of fibers being pulled out) is observed in Figure 6(c), which results in the separation of the reinforcement component from the matrix component. On the other hand, the matrix (resin) and reinforcement (fibers) are well bonded for the 4th specimen[16].

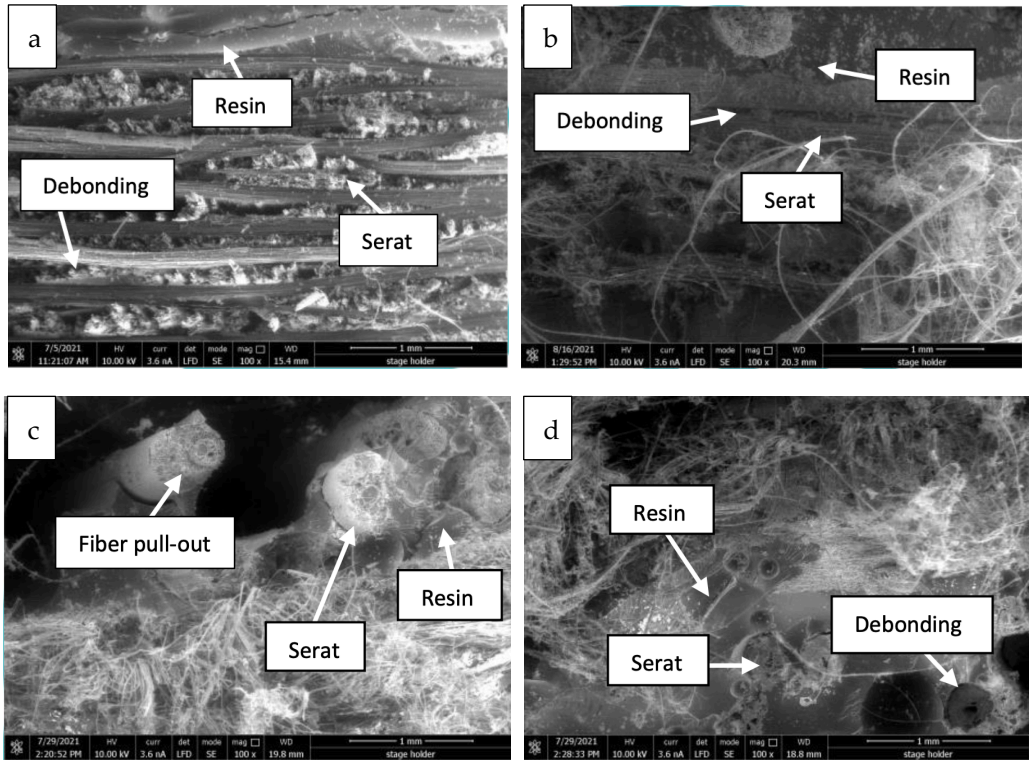

Figure 5. SEM images for all variations (a) 1st variation, (b) 2nd variation, (c) 3rd variation, and (d) 4th variation

3.5 Ballistic Test Analysis

First Variation

The composite material composed of 60% resin, 10% salacca frond fibres, 5% SiC filler, 5% Al_2O_3 filler, 10% carbon fibers, and 10% Kevlar fibers was subjected to ballistic testing using 9 mm caliber ammunition and a P1 Pindad gun at a distance of 5 meters, following NIJ 0101.06 Level II standards. The obtained Back Face Signature (BFS) for 1st variation was 3.79 mm. Since this value is still far below 44 mm, it is very safe and meets Level IIA and II specifications.

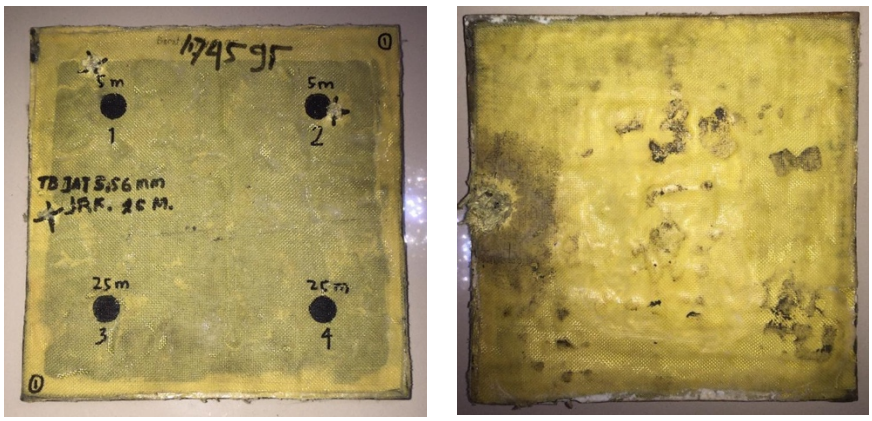

(a) (b)

Figure 6. The ballistic test results for 1st variation (a) Front View, and (b) Back view

Therefore, further testing needs to be conducted for the next level. Level III testing was performed using 5.56x45 mm caliber ammunition, an SS1 rifle, and a distance of 25 meters. The composite material was shot at the lower left part. The result obtained was penetration because it couldn't withstand the impact when the bullet hit, which means it is not safe and doesn't pass the Level III requirements. The ballistic test results can be seen in Figure 6(a) and (b).

Second Variation

The composite material composed of 60% resin, 5% salacca palm fibres, 5% SiC filler, 5% Al_2O_3 filler, 10% carbon fibers, and 15% Kevlar fibers was subjected to ballistic testing using 9 mm ammunition and a P1 Pindad gun at a distance of 5 meters, in accordance with NIJ 0101.06 Level II specifications. The obtained result was non-penetration with a BFS of 9.18 mm, as this BFS value is still well below 44 mm, indicating it is very safe and meets Level IIA and II specifications. Therefore, additional assessment is required for the next level. The level III ballistic testing results are penetrable because the object cannot withstand the impact of the bullet, indicating that it is not secure and does not qualify for level III.

Based on previous research conducted by J. Naveen et al, the natural fiber-based bulletproof vest has a lower indentation depth compared to the Kevlar fiber-based bulletproof vest[17].

The current study shows that the composition of salak frond fiber greatly affects the ballistic strength of the material, where the higher the content of salak frond fiber (in this case from 5% to 10%) will increase the resistance of the composite material to firing loading. This is evidenced by specimens with 10% salak frond fiber content having a minimal BFS of 3.79 mm compared to specimens with 5% salak frond fiber content having a BFS of 9.18 mm. Bulletproof vest materials with more composition of salak frond fibers have lower depth indentation results. In other words, the bulletproof material with lower composition of salak frond fibers obtained 58% higher BFS, but still below the required limit according to the standard of 44 mm[18]. The presence of natural fibers in the form of salak frond fibers in variations 1 and 2 is certainly able to reduce the use of synthetic fibers (kevlar fibers) so that of course it will also reduce production costs where kevlar fibers have a fairly expensive price.

These two specimens succeeded as NIJ level II and IIA standard bullet resistant materials, where the BFS determined according to this NIJ standard is 44 mm. With BFS results that are still far from 44 mm, it is possible that this material will also succeed at level IIIA because it uses a velocity of 430 m/s where the velocity is not too far away from level II of 379 m/s, so it is recommended that further research be carried out with level IIIA testing. Level III testing has also been carried out using a long-barreled shotgun with the results of all specimens penetrating.

The weight of the specimen with a composition of 10% salak frond fiber and 10% kevlar fiber is 1,877.5 g while the weight of the specimen with a composition of 5% salak frond fiber and 15% kevlar fiber is 1,898.7 g, so that from this composition the specimen

with the best ballistic ability has a smaller weight. This is also very efficient for troop mobility when using bulletproof vests.

The results of this ballistic test have a relationship with the results of impact resistance, where specimens that have good ballistic resistance also have good impact resistance.

Third Variation

The composite material composed of 60% resin, 2.5% salak frond fiber, 7.5% SiC filler, 7.5% Al2O3 filler, 2.5% carbon fiber and 20% kevlar fiber were ballistically tested using 9 mm caliber and Pindad P1 pistol with a distance of 5 m referring to NIJ 0101.06 Level II. The results obtained are not penetrated with a BFS of 7.10 mm, because the BFS results obtained are still far from 44 mm which means it is very safe and passes at levels IIA and II. Therefore, additional assessment is required for the next level. The level III ballistic testing results are penetrable because the object cannot withstand the impact of the bullet, indicating that it is not secure and does not qualify for level III.

Fourth Variation

The composite material composed of 60% resin, 2.5% salak frond fiber, 5% SiC filler, 5% Al2O3 filler, 2.5% carbon fiber and 25% kevlar fiber were ballistically tested using a 9 mm caliber and a P1 Pindad pistol with a distance of 5 m which refers to NIJ 0101.06 Level II. The results obtained are not penetrated with a BFS of 6.48 mm, because the BFS results obtained are still far from 44 mm which means it is very safe and passes at levels IIA and II, so it is necessary to test to the next level, namely IIIA but due to limited munitions, testing is carried out to two levels above it, namely level III with a caliber of 5.56x45 mm, SS1 rifle and a distance of 25m. The composite was fired at the top right. The result obtained is penetrated because it cannot withstand the impact when the bullet hits, which means it is not safe and does not qualify for level III.

Based on previous research conducted by Deepak M.V.S et al, it is stated that the addition of ceramic fillers such as SiC and Al_2O_3 to kevlar fibers results in an increase in impact strength values if the composition of kevlar fibers is constant. Kevlar fibers are usually resistant to impact and can resist propagating cracks[19].

The current study shows that when making changes by varying kevlar fibers as well as ceramic fillers (SiC and Al_2O_3), kevlar fibers greatly affect the ballistic strength of the material, where the higher the kevlar fiber content (in this case from 20% to 25%) will increase the resistance of the composite material to firing loading. This is evidenced by specimens with 25% kevlar fiber content having a minimal BFS of 6.48 mm compared to specimens with 20% kevlar fiber content having a BFS of 7.10 mm. Bulletproof vest materials with more kevlar fiber composition have lower depth indentation results. In other words, bullet-resistant materials that have a low kevlar fiber composition obtained 8.73% higher BFS results, but still below the required limit according to the standard of 44 mm. The presence of SiC and Al_2O_3 ceramic fillers can certainly reduce the use of kevlar fibers.

These two specimens succeeded as NIJ level II and IIA standard bullet resistant materials, where the BFS determined according to this NIJ standard is 44 mm. With BFS results that are still far from 44 mm, it is possible that this material will also succeed at level IIIA, so it is recommended that further research be carried out with level IIIA testing. Level III testing has also been carried out using a long-barreled rifle with the results of all specimens penetrating.

The weight of the specimen with a composition of 15% ceramic filler (SiC and Al_2O_3) and 20% kevlar fiber is 2018.7 g while the weight of the specimen with a composition of 10% ceramic filler (SiC and Al_2O_3) and 25% kevlar fiber is 1,885 g, so from this composition the specimen with the best ballistic ability has a smaller weight. This is also very efficient for troop mobility when using bulletproof vests.

The results of this ballistic test have a relationship with the results of impact resistance, where specimens that have good ballistic resistance also have good impact resistance.

4. Conclusions

Based on the results of the analysis that has been carried out, the conclusions that can be drawn are:

a. The Vaccum Assisted Resin Transfer Molding (VARTM) method with a third mold is the best modification because it results in faster resin distribution and manufacturing.
b. The impact strength, tensile strength, hardness, microstructure and ballistic capability of variations 1, 2, 3, and 4 were obtained as follows:
   - The impact strength value in variation 1 (60% resin, 10% salak frond fiber, 5% SiC filler, 5% Al2O3 filler, 10% carbon fiber and 10% kevlar fiber) is 0.19 J/mm², while in variation 2 (60% resin, 5% SiC filler, 5% Al_2O_3 filler, 5% salak frond fiber, 10% carbon fiber and 15% kevlar fiber) is 0.17 J/mm². So variation 1 has an impact strength 10.5% greater than variation 2. The impact strength value in variation 3 (60% resin, 7.5% SiC filler, 7.5% Al_2O_3 filler, 2.5% salak frond fiber, 2.5% carbon fiber and 20% kevlar fiber) is 0.22 J/mm², while in variation 4 (60% resin + 5% SiC filler + 5% Al_2O_3 filler + 2.5% salak frond fiber + 2.5% carbon fiber + 25% kevlar fiber) is 0.34 J/mm². So variation 4 has an impact strength 35.3% greater than variation 3.
   - The hardness value in variation 1 is 22.72 HRF, while the hardness value in variation 2 is 33.12 HRF. So that variation 2 has a hardness 31.4% greater than variation 1. The hardness value in variation 3 is 40.52 HRF, while the hardness value in variation 4 is 49.56 HRF. So that variation 4 has a hardness 18.24% greater than variation 1.
   - The tensile strength value in variation 1 was 148.59 N/mm², the strain was 0.04% and the elastic modulus was 3746.81 N/mm².The tensile strength of variation 2 was 246.93 N/mm², the strain was 0.06% and the elastic modulus was 4355.9 N/mm².So that variation 2 has a tensile strength 39.8% greater than variation 1. While the tensile strength value in variation 3 is 161.16 N/mm², the strain is 0.04% and the elastic modulus is 3779.98 N/mm².The tensile strength value of variation 4 was 177.91 N/mm², strain of 0.06%, elastic modulus of 3190.45 N/mm². So variation 4 has a tensile strength 9.41% greater than variation 3.
   - The BFS results in variation 1 amounted to 3.79 mm with a weight of 1877.5 g, while in variation 2 amounted to 9.18 mm with a weight of 1898.75 g. The BFS values of variations 1 and 2 have met the requirements of the NIJ level II standard,

namely u < 44 mm.BFS results in variation 3 amounted to 7.10 mm, while in variation 4 amounted to 6.48 mm. The BFS values of variations 3 and 4 have met the requirements of the NIJ level II standard. So from variations 1, 2, 3 and 4 the best is variation 4 because it has a smaller weight and BFS value that is still safe.

- SEM test results from variations 1,2,3,4 show that the matrix (resin) and reinforcement (fiber) have bonded well.

Acknowledgments: I am sincerely grateful to Ahmad Adifani and Vernida Mufida for his continuous support and assistance in this research. I would also like to express my heartfelt gratitude to PT Badak NGL academy for their valuable collaboration with PNJ research and teamwork.

References

1. NIJ Standard-0101.06, "Ballistic Resistance of Personal Body Armor," *NIJ Stand.*, p. 89, 2008.
2. L. Lakshmi and C. G. Nandakumar, "Investigations on the Performance of Metallic and Composite Body Armors," *Procedia Technol.*, vol. 25, no. Raerest, pp. 170–177, 2016, doi: 10.1016/j.protcy.2016.08.094.
3. P. K. Mallick, *Materials, Manufacturing, and Design, Third Edition*. 2007.
4. A. B. M. Azhar, M. S. Risby, A. S. M. Sohaimi, M. N. Hafizi, S. Khalis, and S. Asrul, "Conceptual mold design for multi-curved natural fiber reinforced composite body armor panel," *Procedia CIRP*, vol. 37, pp. 95–100, 2015, doi: 10.1016/j.procir.2015.08.017.
5. D. A. N. Serat, K. Dalam, and M. Energi, "Analisis Kemampuan Rompi Anti Peluru Yang Terbuat Dari Komposit Hgm-Epoxy," 2017.
6. S. Rajesh, B. V. Ramnath, and K. O. Praveen, "EasyChair Preprint Experimental Investigation of Mechanical and Machining Characteristics of Aramid-Natural Fiber Composite," 2020.
7. R. Stopforth and S. Adali, "Experimental study of bullet-proofing capabilities of Kevlar, of different weights and number of layers, with 9 mm projectiles," *Def. Technol.*, vol. 15, no. 2, pp. 186–192, 2019, doi: 10.1016/j.dt.2018.08.006.
8. A. M. R. Azmi, M. T. H. Sultan, A. Hamdan, A. F. M. Nor, and K. Jayakrishna, "Flexural and Impact Properties of A New Bulletproof Vest Insert Plate Design Using Kenaf Fibre Embedded with X-Ray Films," *Mater. Today Proc.*, vol. 5, no. 5, pp. 11193–11197, 2018, doi: 10.1016/j.matpr.2018.01.143.
9. A. M. R. Azmi, M. T. H. Sultan, M. Jawaid, and A. F. M. Nor, "A newly developed bulletproof vest using kenaf-X-ray film hybrid composites," *Mech. Phys. Test. Biocomposites, Fibre-Reinforced Compos. Hybrid Compos.*, pp. 157–169, 2018, doi: 10.1016/B978-0-08-102292-4.00009-6.
10. N. M. Nurazzi *et al.*, "A review on natural fiber reinforced polymer composite for bullet proof and ballistic applications," *Polymers (Basel).*, vol. 13, no. 4, pp. 1–42, 2021, doi: 10.3390/polym13040646.
11. V. Yudha, H. S. B. Rochardjo, J. Jamasri, R. Widyorini, F. Yudhanto, and S. Darmanto, "Isolation of cellulose from salacca midrib fibers by chemical treatments," *IOP Conf. Ser. Mater. Sci. Eng.*, vol. 434, no. 1, 2018, doi: 10.1088/1757-899X/434/1/012078.
12. A. Pérez, "No 主観的健康感を中心とした在宅高齢者における 健康関連指標に関する共分散構造分析Title," *BMC Public Health*, vol. 5, no. 1, pp. 1–8, 2017, [Online]. Available: https://ejournal.poltektegal.ac.id/index.php/siklus/article/view/298%0Ahttp://repositorio.unan.edu.ni/2986/1/5624.pdf%0Ahttp://dx.doi.org/10.1016/j.jana.2015.10.005%0Ahttp://www.biomedcentral.com/1471-2458/12/58%0Ahttp://ovidsp.ovid.com/ovidweb.cgi?T=JS&P.
13. M. Hancioglu, E. M. Sozer, and S. G. Advani, "Comparison of in-plane resin transfer molding and vacuum-assisted resin transfer molding 'effective' permeabilities based on mold filling experiments and simulations," *J. Reinf. Plast. Compos.*, vol. 39, no. 1–2, pp. 31–44, 2020, doi: 10.1177/0731684419868015.

14. C. Polowick, *Optimizing Vacuum Assisted Resin Transfer Moulding (VARTM) Processing Parameters to Improve Part Quality*, no. April. 2013.
15. P. Priyanka, A. Dixit, and H. S. Mali, "High strength Kevlar fiber reinforced advanced textile composites," *Iran. Polym. J. (English Ed.*, vol. 28, no. 7, pp. 621–638, 2019, doi: 10.1007/s13726-019-00721-7.
16. W. D. Callister Jr and D. G. Rethwisch, *Characteristics, Application, and Processing of Polymers*. 2018.
17. J. Naveen, K. Jayakrishna, M. T. Bin Hameed Sultan, and S. M. M. Amir, "Ballistic Performance of Natural Fiber Based Soft and Hard Body Armour- A Mini Review," *Front. Mater.*, vol. 7, no. December, pp. 1–6, 2020, doi: 10.3389/fmats.2020.608139.
18. F. S. da Luz, F. da C. G. Filho, M. S. Oliveira, L. F. C. Nascimento, and S. N. Monteiro, "Composites with natural fibers and conventional materials applied in a hard armor: A comparison," *Polymers (Basel).*, vol. 12, no. 9, pp. 1–13, 2020, doi: 10.3390/POLYM12091920.
19. D. Mvs, K. M. Subbaya, T. S. R, A. Chikkala, P. K. Veera Gowda, and S. S. Almos, "Impact Behavior of Hybrid Nano Filled Kevlar Reinforced Composites," no. June, pp. 456–458, 2020.

PT. Mencerdaskan Bangsa Indonesia

PT MENCERDASKAN BANGSA INDONESIA (MBI), 4th Floor Gedung STC Senayan Room 31-34, Jl. Asia Afrika Pintu IX, Jakarta 10270, Indonesia.